Chinese Journal of
POLYMER SCIENCE

RESEARCH ARTICLE

https://doi.org/10.1007/s10118-023-2967-6
Chinese J. Polym. Sci. **2023**, *41*, 1410–1424

Sliding Dynamics of Slide-Ring Polymers Based on the Bead-Spring Model

Zhong-Qiang Xiong and Wei Yu*

Advanced Rheology Institute, Department of Polymer Science and Engineering, State Key Laboratory for Metal Matrix Composite Materials, Shanghai Jiao Tong University, Shanghai 200240, China

Abstract Understanding the sliding dynamics is critical for developing rotaxane-based mechanically interlocked polymers. In this work, we studied the sliding behavior of a sliding ring and its influence on the dynamics of attached polymer chains based on the heterogeneous bead-spring model. The sliding constraint was treated as direction-related confinement with the heterogeneous friction coefficient and constraint intensity. The relaxation spectrum, the diffusion dynamics, and the sliding dynamics under/after drag were studied for typical sliding chain topologies, namely, the sliding dangling chain, the constraint sliding chain, and the sliding strand. Compared with the non-sliding chains (such as the free chain, the dangling chain, and the network strand), the slide of one or two chain ends induces an additional slow process in the transition from the Rouse-type behavior to the long-time terminal behavior. The effect of the sliding-related process on the diffusion of specific chain segments relies on the chain topology. The slow sliding relaxation process is also observed in the sliding process during and after chain deformation, whose characteristic time is at least three times the terminal relaxation time of the free chain with the same length, and will increase with the friction coefficient (*i.e.*, the interaction) between the ring and the polymer axial. The results of this work will benefit the understanding of the sliding dynamics in experiments.

Keywords Sliding chain; Bead-spring model; Heterogeneity; Diffusion; Mean conformation

Citation: Xiong, Z. Q.; Yu, W. Sliding dynamics of slide-ring polymers based on the bead-spring model. *Chinese J. Polym. Sci.* **2023**, *41*, 1410–1424.

INTRODUCTION

Polymeric materials, as a branch of soft matter, have enormous internal microstructures and degrees of freedom. The way that monomers connect to form long chains or network topology significantly influences the dynamic and mechanical properties of polymers. If all the monomers are connected through the covalent bond, multi-scale dynamics and rheology can be well described by the bead-spring dynamics of arbitrary topologies without entanglements[1,2] or tube concept for linear and branched chains with well-defined topologies and sufficient entanglements.[3–5] If some of the covalent bonds are replaced by dynamic bonds, the coupling between reversible association-dissociation and chain dynamics induces additional mechanisms that influence the relaxation and the modulus of polymers.[6,7] If the topological constraints between chains are used to construct a "branching point" that can slide, the usual crosslinked network can be turned into a particular sliding ring network. Fig. 1 shows some chain types in fixed networks and sliding ring networks. A significant consequence of the sliding "branch point" is the dynamic variation of the topological structures of polymer chains and networks. One example of such a sliding ring network can be found in the sliding-ring gels (SRG)[8,9] based on polyrotaxane with cyclodextrin (CD) as the ring and poly(ethylene glycol) (PEG) as the axial.[10,11] A distinctive feature of this new material is its super soft property. Due to sliding rings, molecular chains can adapt to external stimuli by sliding with greater freedom. When a network is deformed, the usual branching points are subjected to a certain amount of tension. However, when the branching point can slide, the chain segment can further adjust the structure by sliding to form a larger deformation, thus reducing the modulus of the material to form a super soft property.[12–14] The other example is the mechanically interlocked networks (MINs) containing a high density of rotaxanes consisting of a crown ether wheel and a dumbbell-shaped secondary ammonium-salt-based axle.[15–18] Integration of the host-guest interaction and the amplification effect of high-density rotaxanes endow the bulk material with excellent toughness and damping capacity. Understanding the sliding dynamics is essential for the design and application of MINs.

To understand such sliding ring dynamics, one can observe the relaxation process at different time scales by rheological or dielectric experiments.[19] For instance, the effect of sliding ring size on relaxation behavior was studied by Kato *et al*.[8,20] Kashiwagi *et al*.[21] studied the contribution of sliding rings to the relaxation behavior at different sliding states (*e.g.*, unrestricted slip rings in the network and free slip rings).

* Corresponding author, E-mail: wyu@sjtu.edu.cn

Special Issue: Theory and Simulation of Macromolecules
Received December 31, 2022; Accepted February 6, 2023; Published online March 23, 2023

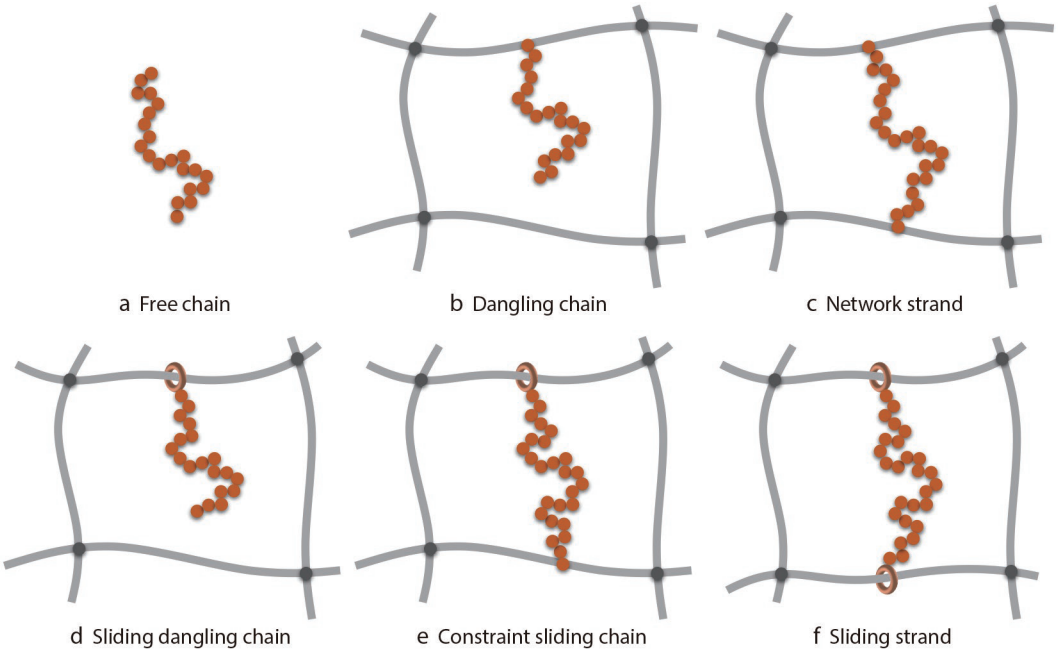

Fig. 1 Free chains (a) and types of chain in fixed networks (b, c) and sliding ring networks (d–f).

However, due to the complexity of structural control in synthesis, the results of macroscopic rheological and dielectric experiments are more of a phenomenological result, and it is challenging to differentiate the sliding motion from segmental dynamics. The molecular dynamics (MD) simulation is a powerful tool to reveal the sliding dynamics because the sliding structure can be precisely constructed. Thus, the sliding characteristics can be obtained by counting the motion of the ring and the molecular chain segments. For example, focusing on the mean square displacement (MSD) of chain segments based on the coarse-grained molecular dynamics (CG-MD) simulations,[22–26] one can investigate the characteristic behavior of the ring sliding process,[22] the sliding process of a small ring on a large polymer circle[23] or through a molecular knot,[24] and the dynamics of a sliding ring chain bound between two rigid rods.[26] In particular, Yasuda *et al*.[27] estimated the sliding modes on a structural unit scale by combining the full atomistic MD simulations with the Quasi-Elastic Neutron Scattering (QENS) experiments. Due to computational complexity, MD approaches are often limited to studying the sliding motions on small spatial and temporal scales.

In contrast to the advances in experiments and computer simulations, the theoretical understanding of sliding chain dynamics is still minimal. On the one hand, this problem involves intermolecular interactions between at least two molecular chains *via* sliding rings, which are often complex van der Waals force interactions.[22] On the other hand, the ring will slide away by external drag *via* a stretching chain, which causes this intermolecular interaction to be a dynamic coupling interaction. There was a continuum model to formulate such sliding dynamics of slide-ring networks[28] based on the transient network theory,[29] where the local dynamics of both ring and chain segments were ignored. In this work, we are more concerned with the detailed dynamic mode of the sliding linear chain based on the bead-spring model and ignore the relaxation mode of the ring structure itself. Thus, the whole ring is treated as a sliding bead. Additionally, the chain is set to slide in a fixed rod (Fig. 2) as a toy model to capture sliding characteristics. The interaction between the sliding ring and the fixed rod is simplified into a linear elastic interaction in the direction perpendicular to the fixed rod, while it is considered free (no interaction) in the direction along the rod. For simplicity, the study in this work limits the structure to the simplest branching structure, the T-like structure, which contains the sliding characteristic of the ring we concern with. The fixed rod simply acts as a sliding confinement incorporated into the Rouse dynamics of linear siding chains. The diffusion of chain segments and the response of rings by dragging of molecular chains are the key clues to study the dynamics and sliding mode of chain segments. The study is organized as follows: in section **Simplification of Sliding Ring**, the sliding ring is simplified into a slidable bead to offer sliding confinement. Based on this proposal, in section **Dynamic Equation with Sliding Confinements**, the anisotropy of the constraints is represented by using different constraint matrices in each of the three coordinates to establish the sliding constraints. Thus, the dynamic equation of the sliding chain is constructed. In section **Relaxation Time Spectrum**, the relaxation spectrum is calculated under the sliding con-

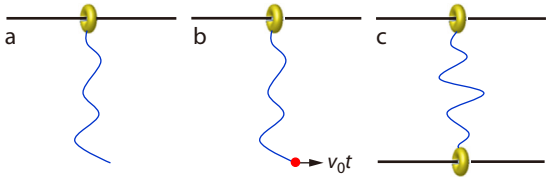

Fig. 2 Linear Rouse chains with a sliding constraint at one end in a fixed rod, (a) the other end is free, (b) the other end is pulled, and (c) the other end is also in a sliding constraint.

https://doi.org/10.1007/s10118-023-2967-6

straints, which govern all relaxation processes. Based on the relaxation spectrum, the diffusion behavior of chain segments and the characteristic transitions of the diffusion are discussed in section **Characteristic Transition of Diffusion Behavior of Chain Segments**. The evolution of the mean conformation of the sliding chain segments by dragging is calculated in section **Evolution of Mean Conformation of Chain**.

SLIDING RING MODEL

Simplification of Sliding Ring

The sliding ring is a special ring-like polymer segment that can slide along a polymer chain. Because of the topological non-crossing requirement, the ring can move freely along the chain, while the ring size limits the maximum displacement in the perpendicular direction. From the other point of view, the polymer axis can thread in and out of the ring, but the lateral movement of segments is limited by the ring size. In this view, the motion of axial segments is reminiscent of reptation in a virtual tube, which describes the dynamics of entangled polymer chains. The difference is that the confinement in the tube model of entangled polymers is continuous at length scales above the tube diameter, while the confinement is localized for several Kuhn segments for slide-ring polymers. Thus, it can be regarded as a weak entanglement effect with a temporary feature for a pairwise interaction, where the interaction dynamically changes with time and may switch to adjacent positions for the next moment. Dealing with this localized, transient interaction is the key to understanding the sliding ring dynamics.

A noticeable feature is the ring size. If the ring size is too small, the strong interaction makes the ring difficult to slide relatively.[22] In contrast, when the ring size is much larger than the tube diameter of entanglements, the weak interaction leads to an insignificant sliding constraint. Therefore, the size of the ring is a crucial parameter for the sliding dynamics. In this work, we will not consider the case that the ring size is much larger than the tube diameter. We are more concerned with the relaxation modes of the linear chain attached to the ring and ignore the relaxation modes of the sliding ring itself. Therefore, the entire ring is treated as a slidable bead regardless of its structure. The interaction between the ring and axial chain can be described by elastic forces, which depend nonlinearly on the ring size and the relative position of the polymer axis in the ring. For smaller rings, this elastic force can be deduced from the nonlinear van der Waals interactions. When the whole system is near equilibrium, the axial chain segment is in equilibrium within the constrained potential field of the ring. Expansion at the equilibrium location always gives a simple harmonic potential, implying that this constraint can be approximated as a Hooke elastic constraint near the equilibrium position. Therefore, A spring constant κ^* is defined to represent the interaction between the ring and axial chain. Thus, a smaller ring induces a stronger interaction and a larger κ^*, and a larger ring leads to a smaller κ^*. Simplifying the sliding ring to a slidable bead makes it possible to formulate the polymer dynamics into a bead-spring model.

Dynamic Equation with Sliding Confinements

To describe the dynamics of linear Rouse chains, we need to determine the time evolution of each bead's position in the molecular chain. Supposing there is a bead-spring chain with a total of n_b beads, the positions of beads are $\boldsymbol{R}(t) = [\boldsymbol{R}(1,t), \boldsymbol{R}(2,t), \cdots, \boldsymbol{R}(n_b,t)]^T$ with the serial number 1 representing the ring and the serial number n_b for the other end. It can be decomposed into three coordinate representations, *i.e.*, $\boldsymbol{R}(t) = [\boldsymbol{x}(t), \boldsymbol{y}(t), \boldsymbol{z}(t)]$ with $\boldsymbol{x}(t) = [x(1,t), x(2,t), \cdots, x(n_b,t)]^T$ and similar expressions for $\boldsymbol{y}(t)$ and $\boldsymbol{z}(t)$. The structures shown in Fig. 2 are three typical scenarios of sliding rings in a network. A linear chain with sliding confinement at one end, as shown in Fig. 2(a), resembles a slidable dangling chain in slide-ring gels (Fig. 1d). Herein, we ignore the motion of the axial chain. We assume the fixed rod of the axial chain is along the x-axis, so the motion of the sliding end in the x-axis direction is free, while the y- and z-axis directions are constrained. Fig. 2(b) shows the case where the other end of the molecular chain has a drag with a constant velocity v_0 towards the positive direction of the x-axis. We can set the point drag at $\overline{\boldsymbol{R}}(n_b,t) = [v_0 t, y_0, 0]$ with confinement intensity κ^+, with the special case $\kappa^+ = 0$ corresponding to the free end in Fig. 2(a). For nonvanishing κ^+, it resembles a constraint sliding chain with one end chemically crosslinked in the network, as in Fig. 1(e). The governing equation for these chains' conformation $\boldsymbol{R}(t)$ is readily from the heterogeneous bead-spring (HBS) model[2,30] by incorporating such sliding confinement introduced in section **Simplification of Sliding Ring**. The HBS model is a generalization of the Rouse model for heterogeneous polymers with arbitrary topology, which is consistent with the same basic assumptions (linear spring and constant friction coefficient near the equilibrium) of the Rouse model but aims at the complex topology and heterogeneity of chains based on Graph Theory and the Maximum Entropy Principle. By using the constraints to manipulate the Rouse chain, the dynamics of a linear chain with sliding restriction can be expressed as

$$k_B T \frac{\partial \ln \psi_x}{\partial \boldsymbol{x}(t)} + \left(\boldsymbol{M}\cdot\boldsymbol{\kappa}\cdot\boldsymbol{M}^T + \overline{\boldsymbol{\kappa}}\big|_{\kappa^*=0}\right)\cdot\boldsymbol{x}(t) + \boldsymbol{\zeta}\cdot\frac{\mathrm{d}\boldsymbol{x}(t)}{\mathrm{d}t} = \overline{\boldsymbol{\kappa}}\big|_{\kappa^*=0}\cdot\overline{\boldsymbol{x}}(t) \quad (1a)$$

$$k_B T \frac{\partial \ln \psi_y}{\partial \boldsymbol{y}(t)} + \left(\boldsymbol{M}\cdot\boldsymbol{\kappa}\cdot\boldsymbol{M}^T + \overline{\boldsymbol{\kappa}}\right)\cdot\boldsymbol{y}(t) + \boldsymbol{\zeta}\cdot\frac{\mathrm{d}\boldsymbol{y}(t)}{\mathrm{d}t} = \overline{\boldsymbol{\kappa}}\cdot\overline{\boldsymbol{y}} \quad (1b)$$

$$k_B T \frac{\partial \ln \psi_z}{\partial \boldsymbol{z}(t)} + \left(\boldsymbol{M}\cdot\boldsymbol{\kappa}\cdot\boldsymbol{M}^T + \overline{\boldsymbol{\kappa}}\right)\cdot\boldsymbol{z}(t) + \boldsymbol{\zeta}\cdot\frac{\mathrm{d}\boldsymbol{z}(t)}{\mathrm{d}t} = \boldsymbol{0} \quad (1c)$$

Eq. (1) represents the balance of elastic force and viscous force at each bead, and the right-hand side of Eq. (1) denotes the imposed constraints. $\overline{\boldsymbol{x}}(t)$ is an n_b dimensional vector, and the $n_b{}^{\text{th}}$ component is the x-component $v_0 t$ of the vector $\overline{\boldsymbol{R}}(n_b,t)$, while the rest of the components are zero. $\overline{\boldsymbol{y}}$ is also an n_b dimensional vector, and the $n_b{}^{\text{th}}$ component is the time-independent y-component y_0 of the vector $\overline{\boldsymbol{R}}(n_b,t)$, while the rest of the components are zero as well. Since the z-component of the vector $\overline{\boldsymbol{R}}(n_b,t)$ is zero, $\overline{\boldsymbol{z}}$ is just an n_b dimensional zero vector. In addition, $\boldsymbol{\zeta}$ and $\overline{\boldsymbol{\kappa}}$ are diagonal matrices of order n_b, denoting the friction coefficient matrix and confinement matrix of the polymer chain. Because there are confinements at the chain end only, $\overline{\boldsymbol{\kappa}}$ has only one or two non-zero elements. $\boldsymbol{M}$ is a structure matrix and $\boldsymbol{M}\cdot\boldsymbol{M}^T$ is known as the Rouse matrix for a linear chain, which describes the linear connection between Kuhn segments. $\boldsymbol{\kappa} = \kappa\boldsymbol{\delta}$ is a diagonal

matrix of order $n_b - 1$ for linear chain describing the stiffness of the polymer chain.[2] Specifically,

$$\boldsymbol{\zeta} = \begin{bmatrix} \zeta_1 & 0 & 0 & 0 & 0 \\ 0 & \zeta_2 & 0 & 0 & 0 \\ 0 & 0 & \zeta_3 & 0 & 0 \\ 0 & 0 & 0 & \cdots & 0 \\ 0 & 0 & 0 & 0 & \zeta_{n_b} \end{bmatrix}_{n_b \times n_b},$$

$$\overline{\boldsymbol{\kappa}} = \begin{bmatrix} \kappa^* & 0 & 0 & 0 & 0 \\ 0 & 0 & 0 & 0 & 0 \\ 0 & 0 & \cdots & 0 & 0 \\ 0 & 0 & 0 & 0 & 0 \\ 0 & 0 & 0 & 0 & \kappa^+ \end{bmatrix}_{n_b \times n_b}, \quad (2)$$

$$\boldsymbol{M} = \begin{bmatrix} -1 & 0 & 0 & 0 \\ +1 & -1 & 0 & 0 \\ 0 & +1 & \cdots & 0 \\ 0 & 0 & \cdots & -1 \\ 0 & 0 & 0 & +1 \end{bmatrix}_{n_b \times (n_b - 1)}$$

Note that ζ_u is the friction coefficient for u^{th} bead, and it could be different due to the chemical heterogeneity of the chain. In the following, we will consider that the friction coefficient of the ring ζ_1 differs from the rest of the chain beads ζ_u, which are all identical to ζ (a homopolymer chain). The $\kappa^* = 0$ in the x-component equation (Eq. 1a) indicates that the bead $\boldsymbol{R}(1, t)$ is released from the constraint and can move freely along the x-axis as a sliding end, while this bead is constrained at the zero point of the y- and z-axis with constraint intensity κ^*. Therefore, the bead $\boldsymbol{R}(1, t)$ can only slide along the fixed rod, which imitates the sliding constraint. By the way, a planar sliding constraint can also be defined in a similar way when $\kappa^* = 0$ lies in two dimensions but nonvanishing κ^* in the third dimension. For the case of two sliding rods, one can choose $\kappa^+ = \kappa^*$ such that Eq. (1) defines the sliding ring system shown in Fig. 2(c), corresponding to the sliding strand in Fig. 1(f). In this case, $\kappa^+ = \kappa^* = 0$ in the x-axis direction, which means that the two sliding beads are free to slide in x-axis direction. k_B and T in Eq. (1) are the Boltzmann constant and the reference temperature of the system, respectively. The continuity equation is separated by coordinates as well. By setting the conformational distribution function $\psi = \psi_x \psi_y \psi_z$ in the continuity equation, the vanishing coefficients of $\psi_y \psi_z$, $\psi_x \psi_z$ and $\psi_x \psi_y$ lead to

$$\frac{\partial \psi_x}{\partial t} + \frac{\partial}{\partial \boldsymbol{x}(t)} \cdot \left(\frac{d\boldsymbol{x}(t)}{dt} \psi_x \right) = 0 \quad (3a)$$

$$\frac{\partial \psi_y}{\partial t} + \frac{\partial}{\partial \boldsymbol{y}(t)} \cdot \left(\frac{d\boldsymbol{y}(t)}{dt} \psi_y \right) = 0 \quad (3b)$$

$$\frac{\partial \psi_z}{\partial t} + \frac{\partial}{\partial \boldsymbol{z}(t)} \cdot \left(\frac{d\boldsymbol{z}(t)}{dt} \psi_z \right) = 0 \quad (3c)$$

Eqs. (1) and (3) in the direction of each axis have the same form as the HBS model.[2,30] Therefore, we can use the same conclusion for each axis direction. We can introduce the normal coordinate system $\mathcal{R}(p, t) = [\mathcal{X}(p, t), \mathcal{Y}(p, t), \mathcal{Z}(p, t)]$ defined by relations:

$$\boldsymbol{x}(t) = \boldsymbol{\zeta}^{-1/2} \cdot \boldsymbol{V}^x \cdot \mathcal{X}(t) \quad (4a)$$

$$\boldsymbol{y}(t) = \boldsymbol{\zeta}^{-1/2} \cdot \boldsymbol{V}^y \cdot \mathcal{Y}(t) \quad (4b)$$

$$\boldsymbol{z}(t) = \boldsymbol{\zeta}^{-1/2} \cdot \boldsymbol{V}^z \cdot \mathcal{Z}(t) \quad (4c)$$

where $\mathcal{X}(t) = [\mathcal{X}(1, t), \mathcal{X}(2, t), \cdots, \mathcal{X}(n_b, t)]^T$ and similar expressions for $\mathcal{Y}(t)$ and $\mathcal{Z}(t)$. The transformation is determined by the orthogonal matrix $\boldsymbol{V}^r$, $(r = x, y, z)$ respectively from the eigen equations:

$$\boldsymbol{G}_x \cdot \boldsymbol{V}^x = \boldsymbol{V}^x \cdot \boldsymbol{\Lambda}_x$$
$$\text{with } \boldsymbol{G}_x = \boldsymbol{\zeta}^{-1/2} \cdot \left(\boldsymbol{M} \cdot \boldsymbol{\kappa} \cdot \boldsymbol{M}^T + \overline{\boldsymbol{\kappa}}\big|_{\kappa^*=0} \right) \cdot \boldsymbol{\zeta}^{-1/2} \quad (5a)$$

$$\boldsymbol{G}_y \cdot \boldsymbol{V}^y = \boldsymbol{V}^y \cdot \boldsymbol{\Lambda}_y$$
$$\text{with } \boldsymbol{G}_y = \boldsymbol{\zeta}^{-1/2} \cdot \left(\boldsymbol{M} \cdot \boldsymbol{\kappa} \cdot \boldsymbol{M}^T + \overline{\boldsymbol{\kappa}} \right) \cdot \boldsymbol{\zeta}^{-1/2} \quad (5b)$$

$$\boldsymbol{G}_z \cdot \boldsymbol{V}^z = \boldsymbol{V}^z \cdot \boldsymbol{\Lambda}_z$$
$$\text{with } \boldsymbol{G}_z = \boldsymbol{\zeta}^{-1/2} \cdot \left(\boldsymbol{M} \cdot \boldsymbol{\kappa} \cdot \boldsymbol{M}^T + \overline{\boldsymbol{\kappa}} \right) \cdot \boldsymbol{\zeta}^{-1/2} \quad (5c)$$

Then, Eqs. (1) and (3) can be transformed into the eigenmodes equations:

$$\frac{\partial \langle f \rangle_x}{\partial t} = k_B T \left\langle \frac{\partial^2 f}{\partial \mathcal{X}^2(p, t)} \right\rangle_x - \lambda_p^x \left\langle \mathcal{X}(p, t) \frac{\partial f}{\partial \mathcal{X}(p, t)} \right\rangle_x + \zeta_{n_b}^{-1/2} V_{n_b p}^x \kappa^+ v_0 t \left\langle \frac{\partial f}{\partial \mathcal{X}(p, t)} \right\rangle_x \quad (6a)$$

$$\frac{\partial \langle f \rangle_y}{\partial t} = k_B T \left\langle \frac{\partial^2 f}{\partial \mathcal{Y}^2(p, t)} \right\rangle_y - \lambda_p^y \left\langle \mathcal{Y}(p, t) \frac{\partial f}{\partial \mathcal{Y}(p, t)} \right\rangle_y + \zeta_{n_b}^{-1/2} V_{n_b p}^y \kappa^+ y_0 \left\langle \frac{\partial f}{\partial \mathcal{Y}(p, t)} \right\rangle_y \quad (6b)$$

$$\frac{\partial \langle f \rangle_z}{\partial t} = k_B T \left\langle \frac{\partial^2 f}{\partial \mathcal{Z}^2(p, t)} \right\rangle_z - \lambda_p^z \left\langle \mathcal{Z}(p, t) \frac{\partial f}{\partial \mathcal{Z}(p, t)} \right\rangle_z \quad (6c)$$

where $\langle \cdot \rangle_r = \int_\Omega (\cdot) \psi_r dV$ are conformational averages, and λ_p^r are the diagonal components of the diagonal matrix $\boldsymbol{\Lambda}_r$, called the eigenvalues of the matrix $\boldsymbol{G}_r$, $(r = x, y, z; p = 1, 2, \cdots, n_b)$. If $\kappa^+ = 0$ (denoting the free end case in Fig. 2a), there is one and only one zero eigenvalue $\lambda_{p^*}^x = 0$, being the solution of Eq. 5(a) with the normalized eigenvector:

$$\boldsymbol{V}_{p^*}^x = \frac{\boldsymbol{\zeta}^{1/2} \cdot \boldsymbol{1}}{\left| \boldsymbol{\zeta}^{1/2} \cdot \boldsymbol{1} \right|} \quad (7)$$

where $\boldsymbol{1}$ is a vector of order n_b, whose components are all one. If $\kappa^+ \neq 0$, it corresponds to the dragging case in Fig. 2(b). It has been proven that $\lambda_p^r = 0$ is impossible for any eigenvalue if the confinement matrix $\overline{\boldsymbol{\kappa}}$ is nonzero. Therefore, we have $\lambda_p^y = \lambda_p^z \neq 0$ because there is confinement in the y and z directions.

RESULTS AND DISCUSSION

Relaxation Time Spectrum

First, we compare the relaxation time spectrum of different types of chains in fixed networks and sliding ring networks (Fig. 1). The relaxation time is defined as $\tau_p^r = 1/(2\lambda_p^r)$, $(r = x, y, z; p = 1, 2, \cdots, n_b)$, which is determined from Eq. (5). $\tau_p^x = \tau_p^y = \tau_p^z$ represents the threefold degeneracy for each mode if there is no sliding. For typical chains in fixed networks, the relaxation time spectrum of the chain whose ends are under constraint or not is shown in Fig. 3(a). Here we define a time unit $\tau_0 = \zeta/\kappa$, which is about eight times larger than the relaxation

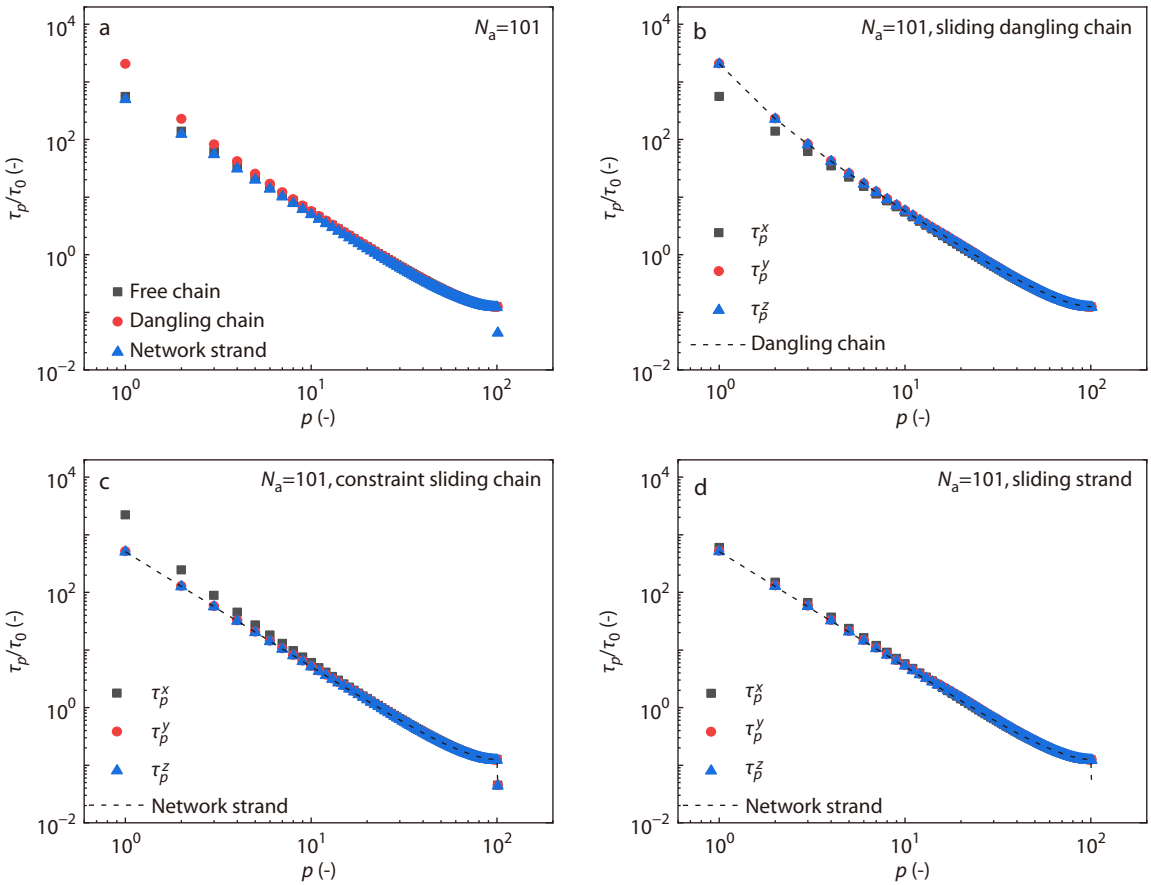

Fig. 3 The relaxation time spectrum of different types of chains in fixed networks (a) and sliding ring networks in Fig. 1 for (b)sliding dangling chain, (c) constraint sliding chain, and (d) sliding strand. The shortest relaxation time in Figs. 3(a) and 3(c) seems quite different because we chose the constraint intensity of the chemical crosslink point as $\kappa^+/\kappa^* = 10$.

time of the fast relaxation mode since the Rouse spectrum is $\tau_p = \dfrac{\tau_0}{8\sin^2(p\pi/2n_b)}$. If the chain whose ends are in sliding confinements, the relaxation time spectrum is split into two parts, τ_p^x and $\tau_p^y = \tau_p^z$, for each type of sliding chain in Fig. 2. Note that the difference in the relaxation time spectrum originates from the value of κ^* and κ^+. The results in Fig. 3 correspond to the constraint intensity of the chemical crosslink point with $\kappa^+/\kappa^* = 10$. The results show that the sliding dangling chain (Fig. 3b) contains the relaxation features of both free chains (in the sliding direction) and dangling chains (in other directions). The constraint sliding chain (Fig. 3c) contains the relaxation features of both dangling chains (in the sliding directions) and network strands (in the other directions). The sliding strand (Fig. 3d) contains the relaxation features of both free chains (in the sliding direction) and network strands (in the other directions). From Eq. (6), the relaxation time spectrum controls the dynamics of the chain and is the basis for understanding the diffusion of chain segments and the response of rings by dragging of molecular chains.

Characteristic Transition of Diffusion Behavior of Chain Segments

As a group of Brownian particles, the positions of the beads in the sliding chain fluctuate continuously, causing the diffusion of the beads. We can use the mean-square displacement (MSD) of beads to characterize the diffusion behavior of the chain segments (Kuhn units). The diffusion behavior for chain segments in the presence of drag constraints is governed by the constraint points whose MSD tends to be constant. Thus, the diffusion behavior in the case of the free end (Fig. 2a) is mainly considered in this section. The typical diffusion behavior can be calculated for each bead u in the linear chain and the center-of-mass of the linear chain, where the MSD can be expressed respectively as

$$\begin{aligned}\mathrm{MSD}(u,t) &= \left\langle (\boldsymbol{R}(u,t) - \boldsymbol{R}(u,0))^2 \right\rangle \\ &= \sum_{r=x,y,z} \left[\left\langle r^2(u,t) \right\rangle_r + \left\langle r^2(u,0) \right\rangle_r - 2\langle r(u,t)\, r(u,0) \rangle_r \right]\end{aligned} \tag{8a}$$

$$\begin{aligned}\mathrm{MSD}_c(t) &= \left\langle (\boldsymbol{R}_c(t) - \boldsymbol{R}_c(0))^2 \right\rangle \\ &= \frac{1}{n_b^2} \sum_{u=1}^{n_b} \sum_{v=1}^{n_b} \sum_{r=x,y,z} \begin{bmatrix} \langle r(u,t)\, r(v,t) \rangle_r + \langle r(u,0)\, r(v,0) \rangle_r \\ -\langle r(u,t)\, r(v,0) \rangle_r - \langle r(u,0)\, r(v,t) \rangle_r \end{bmatrix}\end{aligned} \tag{8b}$$

where $\boldsymbol{R}_c(t) = n_b^{-1} \sum_{u=1}^{n_b} \boldsymbol{R}(u,t)$. Therefore, it is necessary to find the solutions of quantities $\langle r(u,t)\, r(v,t) \rangle_r$ and $\langle r(u,t)\, r(v,0) \rangle_r$. First considering $r = x$ component, use Eq. (4a):

https://doi.org/10.1007/s10118-023-2967-6

$$x(u,t) = \zeta_u^{-1/2} \sum_{p=1}^{n_b} V_{up}^x \mathcal{X}(p,t) \tag{9}$$

Thus,

$$\langle x(u,t)\, x(v,t)\rangle_x = \zeta_u^{-1/2}\zeta_v^{-1/2} \sum_{p=1}^{n_b}\sum_{q=1}^{n_b} V_{up}^x V_{vq}^x \langle \mathcal{X}(p,t)\, \mathcal{X}(q,t)\rangle_x \tag{10a}$$

$$\langle x(u,t)\, x(v,0)\rangle_x = \zeta_u^{-1/2}\zeta_v^{-1/2} \sum_{p=1}^{n_b}\sum_{q=1}^{n_b} V_{up}^x \cdot V_{vq}^x \langle \mathcal{X}(p,t)\, \mathcal{X}(q,0)\rangle_x \tag{10b}$$

Because two different modes are independent on each other, we have $\langle \mathcal{X}(p,t)\, \mathcal{X}(q,t)\rangle_x = \delta_{pq}\left\langle \mathcal{X}^2(p,t)\right\rangle_x$. Let $f = \mathcal{X}^2(p,t)$ and substitute it into Eq. (6a) (details in **Appendix**), we obtain the MSD of bead u (from the definition in Eq. 8a) as:

$$\left\langle (x(u,t) - x(u,0))^2\right\rangle_x = \frac{2k_BT}{\mathrm{tr}(\boldsymbol{\zeta})}t + \zeta_u^{-1}\sum_{p=1,p\neq p^*}^{n_b} V_{up}^x V_{up}^x \left(\left\langle \mathcal{X}^2(p,0)\right\rangle_x \left(1 - e^{-\lambda_p^x t}\right)^2 + \frac{k_BT}{\lambda_p^x}\left(1 - e^{-2\lambda_p^x t}\right)\right) \tag{11}$$

If time t is sufficiently small, $e^{-\lambda_p^x t} \sim 1 - \lambda_p^x t$, so we have

$$\left\langle (x(u,t) - x(u,0))^2\right\rangle_x = \frac{2k_BT}{\zeta_u}t \tag{12a}$$

This result is obtained by neglecting the inertial forces. When considering the inertial force of the chain segment, the MSD will be expressed as a quadratic relation in time for a short time because there is a reversible behavior due to the inertial dominance $\left\langle (x(u,t) - x(u,0))^2\right\rangle_x = (\dot{x}t)^2$. For large enough time t when inertia becomes unimportant, the second term on the right side of Eq. (11) tends to be a constant and much smaller than the first term. So that the MSD in the x-axis direction has asymptotic behavior

$$\left\langle (x(u,t) - x(u,0))^2\right\rangle_x = \frac{2k_BT}{\mathrm{tr}(\boldsymbol{\zeta})}t \tag{12b}$$

Similarly, considering the y- and z-axis components and using Eqs. (4b) and (4c), we have

$$y(u,t) = \zeta_u^{-1/2}\sum_{p=1}^{n_b} V_{up}^y \mathcal{Y}(p,t) \tag{13a}$$

$$z(u,t) = \zeta_u^{-1/2}\sum_{p=1}^{n_b} V_{up}^z \mathcal{Z}(p,t) \tag{13b}$$

By definition Eq. (8a) and using the dynamic modes (details in **Appendix**), we get

$$\left\langle (y(u,t) - y(u,0))^2\right\rangle_y = \zeta_u^{-1}\sum_{p=1}^{n_b} V_{up}^y V_{up}^y \left(\left\langle \mathcal{Y}^2(p,0)\right\rangle_y \left(1 - e^{-\lambda_p^y t}\right)^2 + \frac{k_BT}{\lambda_p^y}\left(1 - e^{-2\lambda_p^y t}\right)\right) \tag{14a}$$

$$\left\langle (z(u,t) - z(u,0))^2\right\rangle_z = \zeta_u^{-1}\sum_{p=1}^{n_b} V_{up}^z V_{up}^z \left(\left\langle \mathcal{Z}^2(p,0)\right\rangle_z \left(1 - e^{-\lambda_p^z t}\right)^2 + \frac{k_BT}{\lambda_p^z}\left(1 - e^{-2\lambda_p^z t}\right)\right) \tag{14b}$$

For time t sufficiently small, there is

$$\left\langle (y(u,t) - y(u,0))^2\right\rangle_y = \left\langle (z(u,t) - z(u,0))^2\right\rangle_z = \frac{2k_BT}{\zeta_u}t \tag{15}$$

which tends to the mean square end-to-end distance of the molecular chains (as shown in the dangling chain in Fig. 4) for time t large enough.

In summary, by definition Eq. (8a) with Eq. (11) and Eq. (14) together, we get

$$\mathrm{MSD}(u,t) = \frac{2k_BT}{\mathrm{tr}(\boldsymbol{\zeta})}t + \sum_{p=1,p\neq p^*}^{n_b} \zeta_u^{-1} V_{up}^x V_{up}^x \frac{k_BT}{\lambda_p^x}\left(1 - e^{-2\lambda_p^x t}\right) + \sum_{p=1}^{n_b} \zeta_u^{-1} V_{up}^y V_{up}^y \frac{k_BT}{\lambda_p^y}\left(1 - e^{-2\lambda_p^y t}\right) + \sum_{p=1}^{n_b} \zeta_u^{-1} V_{up}^z V_{up}^z \frac{k_BT}{\lambda_p^z}\left(1 - e^{-2\lambda_p^z t}\right) \tag{16a}$$

here we are particularly interested in the initial condition with the constrained end $\left\langle \mathcal{X}^2(p,0)\right\rangle_x = \left\langle \mathcal{Y}^2(p,0)\right\rangle_y = \left\langle \mathcal{Z}^2(p,0)\right\rangle_z = 0$. Similarly for the MSD of the center-of-mass of the chain, marking $\beta_p^r = \left(\sum_{u=1}^{n_b} \zeta_u^{-1/2} V_{up}^r\right)^2 / n_b^2$, we have $\beta_{p^*}^x = 1/\mathrm{tr}(\boldsymbol{\zeta})$ by using Eq. (7). Therefore,

$$\mathrm{MSD}_c(t) = \frac{2k_BT}{\mathrm{tr}(\boldsymbol{\zeta})}t + \sum_{p=1,p\neq p^*}^{n_b} \beta_p^x \frac{k_BT}{\lambda_p^x}\left(1 - e^{-2\lambda_p^x t}\right) + \sum_{p=1}^{n_b} \beta_p^y \frac{k_BT}{\lambda_p^y}\left(1 - e^{-2\lambda_p^y t}\right) + \sum_{p=1}^{n_b} \beta_p^z \frac{k_BT}{\lambda_p^z}\left(1 - e^{-2\lambda_p^z t}\right) \tag{16b}$$

The asymptotic behaviors of diffusion for each bead u from Eq. (16a) and the center-of-mass of the chain from Eq. (16b) are

$$\mathrm{MSD}(u,t) = \begin{cases} \dfrac{6k_BT}{\zeta_u}t, & t \ll \tau_0 \\ \dfrac{2k_BT}{\mathrm{tr}(\boldsymbol{\zeta})}t, & t \gg n_b^2\tau_0 \end{cases} \tag{17a}$$

$$\mathrm{MSD}_c(t) = \begin{cases} \dfrac{6k_BT\,\mathrm{tr}\left(\boldsymbol{\zeta}^{-1}\right)}{n_b^2}t, & t \ll \tau_0 \\ \dfrac{2k_BT}{\mathrm{tr}(\boldsymbol{\zeta})}t, & t \gg n_b^2\tau_0 \end{cases} \tag{17b}$$

where ζ_u is the friction coefficient of the u^{th} bead and $\mathrm{tr}(\boldsymbol{\zeta})$ is the friction coefficient of the whole chain. When the time is short enough, the chain segments have the diffusion behavior of free Brownian particles in three-dimension space. When the time is long enough, the diffusion behavior of each chain segment will tend to the diffusion behavior of the whole chain in one-dimension along the fixed axial rod. When $\boldsymbol{\zeta} = \zeta\boldsymbol{\delta}$, we have the diffusion coefficient at a short time three times larger than that at a large time from Eq. (17b), which implies the transition of the chain's diffusion from three-dimension to one-dimension.

To calculate the transition of the diffusion behavior of each bead and the center-of-mass in the middle of two limiting cases, Eqs. (16a) and (16b) are used directly. The results of MSD and $n = \mathrm{dlog}(\mathrm{MSD})/\mathrm{dlog}(t)$ are shown in Fig. 4 for beads at different positions and in Fig. 5(a) for the center of mass. The asymptotic diffusion behaviors of sliding dangling chains at the limiting long and short time are consistent with Eq. (17) for each bead u and the center of mass, respectively. In the intermediate time, the MSD appears with two distinct characteristic processes around the scale of the mean square radius of gyration R_g of the whole chain, which can be clearly seen from the variation of n. This feature is not affected by the specific friction coefficient and constraint intensity (Fig.

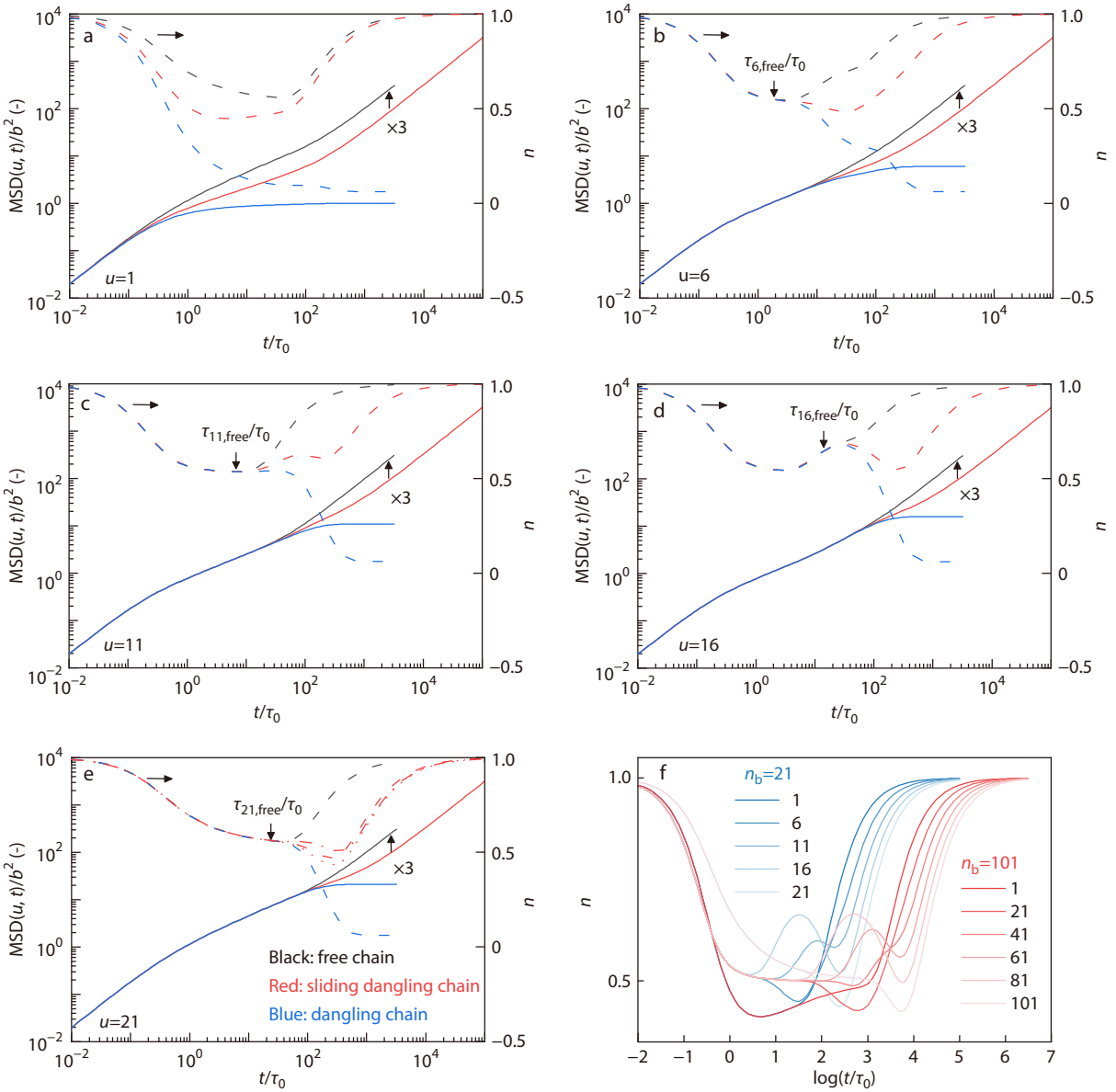

Fig. 4 MSD and n = dlog (MSD) /dlog (t) versus time for different beads u in a free chain (black), a dangling chain (blue) and a sliding dangling chain (red) with n_b = 21. The sliding dangling chain has ζ_1/ζ = 1 and κ^*/κ = 1. (a) u = 1, (b) u = 6, (c) u = 11, (d) u = 16, (e) u = 21, (f) n versus time of sliding dangling chains with n_b = 21 (blue) and n_b = 101 (red). The dot line in (e) represents ζ_1/ζ = 5, κ^*/κ = 1. The dash-dot line in (e) represents ζ_1/ζ = 1, κ^*/κ = 0.2.

4e).

Compared with the diffusion behavior of the end of free chains (black curves in Figs. 4a and 4e), the diffusion behavior of the sliding ring in a sliding dangling chain has a smaller diffusion coefficient in one dimension. The MSD curves of intermediate beads in the free chain, sliding dangling chain, and dangling chain overlap before $\tau_{u,free}/\tau_0$ and exhibit a clear 1/2 scaling, typical of the Rouse relaxation process, which is shown from one Kuhn unit scale to the mean square end-to-end distance scale. Thus, the chain segment cannot feel the constraining from the constraint end below the time scale of $\tau_{u,free}/\tau_0$. At longer time scale (and larger spatial scale from the mean square end-to-end distance to the extended chain size), the chain segments at this stage gradually feel the constraining effect brought by the sliding ring along the molecular chain. So, the diffusion of individual beads differs from each other and depends on the distance from the ring constraint. Due to the sliding constraint, the time of transition to free diffusion becomes longer for inner chain segments and increases with the distance from the sliding ring. As the distance to the ring (equivalently, u) increases, this second transition time increases monotonically without saturation (see n_b = 21 and 101 in Fig. 4f). Such propagation of the sliding confinement along the chain is different from the free chain, where the middle segments enter free diffusion earlier than the ends. It is worth mentioning that the influence of the sliding ring on the movement of the branch chain segments is much more significant than its effect on the movement of the

https://doi.org/10.1007/s10118-023-2967-6

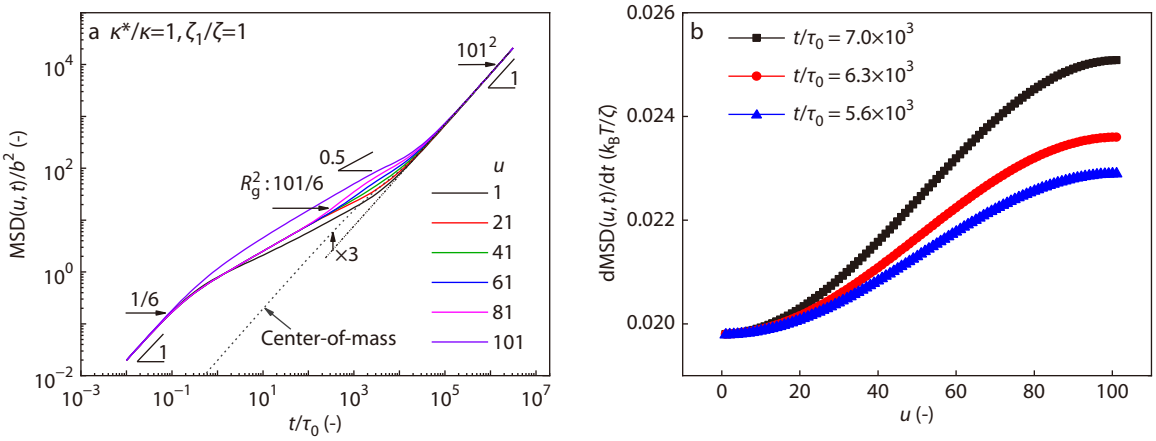

Fig. 5 (a) MSD versus time for a longer sliding dangling chain (n_b = 101); (b) The time derivative of MSD at different positions of the polymer chain.

polymer axial, where only 6–10 structure units near the sliding ring can be affected.[27] As a comparison, we calculated the variation of the MSD of the chain segment with time when one end is fully fixed (*i.e.*, dangling chain). Due to the presence of fixed constraints, the MSD of the chain segment eventually converges to the free chain mean square end-to-end distance with time, as shown in blue curves in Fig. 4. Meanwhile, the MSD of all beads in the dangling chain approaches constants almost simultaneously, indicating that the transition from Rouse regime (n = 0.5) to the confined state (n = 0) is also different from the sliding dangling chain. Therefore, both the sliding confinement and the fixed confinement at the chain end will be active above the time scale of $\tau_{u,\mathrm{free}}/\tau_0$ for the u^{th} bead. In contrast to the fixed confinement of the chain end, the constraining effect of the sliding dangling chain exhibits a unique propagation to the free chain end, which postpones the transition time of all beads to the free diffusion, eventually leading to a threefold decrease in the free diffusion coefficient because the three-dimensional free diffusion has been constrained in one dimension due to the sliding ring.

To quantitatively demonstrate the effect of sliding rings on the motion of molecular chains, the instantaneous diffusion coefficient of each bead is expressed by the derivative of the MSD with respect to time. The MSD and variation of this instantaneous diffusion coefficient along the molecular chain in the second transition regime are shown for a longer chain (n_b = 101) in Fig. 5(a) and Fig. 5(b), respectively. The chain segment close to the sliding ring (u = 1) has a diffusion coefficient close to that of the ring, indicating the obvious influence of the sliding confinement, while the diffusion coefficient is close to that of the free end when the chain segment is close to the free end (u = 101). The diffusion coefficient shows an "S" shaped curve, indicating a gradual transition from the sliding ring to the free end along the molecular chain with increasing motility. It is worth noting that the motility of each bead is time-dependent, and the diffusion coefficients of all chain segments from the sliding ring to the free end will eventually converge for a long time to the one-dimensional diffusion of the chain (Fig. 5a).

The above analysis of the diffusion behavior of the sliding dangling chain can be extended to other sliding chains in Fig. 1. For the molecular chain with sliding constraints at both ends, $\kappa^+ = \kappa^*$ makes Eq. (1) define the system as shown in Fig. 2(c). The constraint matrix of Eq. (1a) now is a zero matrix, and the motion of the molecular chain is therefore not affected by the dragging velocity v_0, so the whole molecular chain behaves like a free chain in the x-axis direction. Similarly, to find the MSD of each bead, the modes in the x-axis direction remain as Eqs. (26) and (29) (**Appendix** A) for sufficiently short or long times, as shown in Eqs. (12a) and (12b), respectively. The modes in the z-axis direction are still Eqs. (32b) and (34b) (**Appendix** A), while the difference lies in that the eigenvalues and eigenvectors need to be recalculated by the new constraint $\kappa^+ = \kappa^*$ at this point. However, for the y-axis direction, due to the distance of the two constraints from each other at y_0, the equations are no longer Eqs. (32a) and (34a) but become

$$\frac{\partial\langle \mathcal{Y}^2(p,t)\rangle_y}{\partial t} = -2\lambda_p^y\langle \mathcal{Y}^2(p,t)\rangle_y + 2k_BT + 2\zeta_{n_b}^{-1/2}V_{n_bp}^y\kappa^* y_0\langle \mathcal{Y}(p,t)\rangle_y \tag{18a}$$

$$\frac{\partial\langle \mathcal{Y}(p,t)\,\mathcal{Y}(q,0)\rangle_y}{\partial t} = -\lambda_p^y\langle \mathcal{Y}(p,t)\,\mathcal{Y}(q,0)\rangle_y + \zeta_{n_b}^{-1/2}V_{n_bp}^y\kappa^* y_0\langle \mathcal{Y}(q,0)\rangle_y \tag{18b}$$

In addition, there is $\langle \mathcal{Y}(p,t)\,\mathcal{Y}(q,t)\rangle_y = \langle \mathcal{Y}(p,t)\rangle_y\langle \mathcal{Y}(q,t)\rangle_y$ for $p \neq q$ if there are constraints, where $\langle \mathcal{Y}(p,t)\rangle_y$ is determined by Eq. (24b) with condition $\kappa^+ = \kappa^*$. Thus, based on the definition, $\left\langle (y(u,t)-y(u,0))^2\right\rangle_y$ can be obtained by a lengthy but explicit calculation. As an asymptotic analysis at a large enough time t, $\left\langle (y(u,t)-y(u,0))^2\right\rangle_y$ converges to a specific constant related to the mean square radius of gyration of the molecular chain under confined conditions. Similarly, the three-dimension diffusion is constrained by the double slide rod to behave as a one-dimension diffusion, since the MSD in the x-axis direction is much larger than the other two directions due to the free diffusion in the long-time condition. Furthermore, when the time t is sufficiently small, it can be verified that the diffusion behavior remains as in Eq. (15) even when the molecular chains have an average orientation stretch. Therefore, in the sliding system shown in Fig. 2(c), the

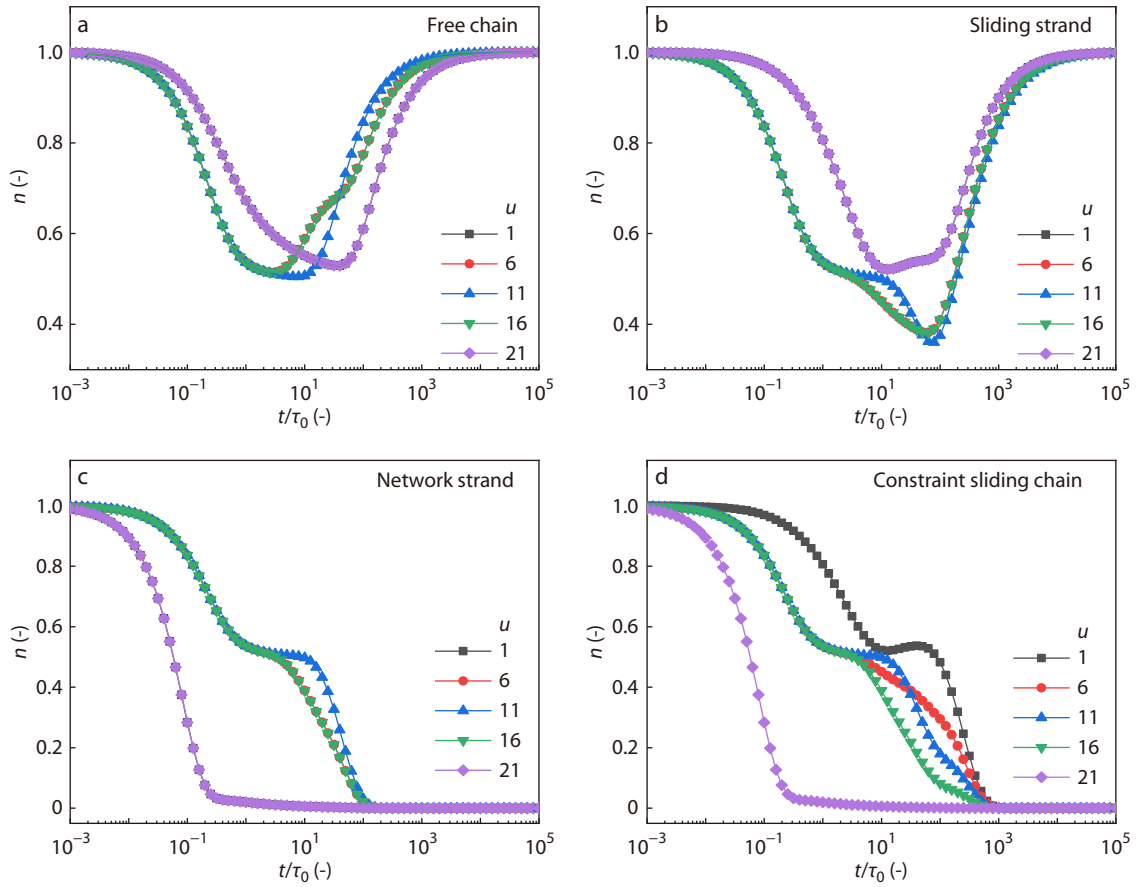

Fig. 6 Scaling exponent n versus time for different beads u in a free chain (a), sliding strand (b), network strand (c), and constraint sliding strand (d). The chain length in the calculation is $n_b = 21$. The friction coefficient and constraint intensity of the sliding ring are $\zeta_1/\zeta = 5$, $\kappa^*/\kappa = 1$, respectively, and the constraint intensity of the chemically crosslink point is $\kappa^+/\kappa = 10$.

conclusion of Eq. (17) still holds.

For comparison, we also calculated the variation of the scaling $n = \mathrm{dlog(MSD)}/\mathrm{dlog}(t)$ of the chain segment with time, and the results are shown in Fig. 6 for the free chain, sliding strand, network strand, and constraint sliding strand (illustrated in Fig. 1). If there is any fixed constraint (such as the network strand in Fig. 6c and constraint sliding chain in Fig. 6d), the scaling n eventually tends to be zero indicating that the diffusion of the whole chain is restricted. Otherwise, the scaling n eventually becomes one for free diffusion (see the free chain in Fig. 6a and the sliding strand in Fig. 6b). Due to the presence of fixed rods for the sliding strand, the mobility of the inner chain segments is restricted in comparison with the free chain, where the region of $n < 1/2$ appears. If one end of the network strand is released by the sliding confinement, *i.e.*, constraint sliding chain, the diffusion behavior of the sliding ring is similar to that of the sliding strand up to the time scale at which the MSD reaches the mean square end-to-end distance of the free chain. The role of the sliding ring can be revealed more clearly by comparing the sliding dangling chain (Fig. 4f), the sliding strand (Fig. 6b), and the constraint sliding chain (Fig. 6d). In contrast to the propagation of the sliding constraint from the ring to the free end in the sliding dangling chain (Fig. 4f), the propagation happens simultaneously from two sliding ends in the sliding strand (Fig. 6b), resulting in the slowest transition to the free diffusion in the middle of the chain. When one end is fixed and the other is sliding (constraint sliding chain, Fig. 6d), the mobility decreases as the distance to the sliding ring increases, but the transition to the cessation of diffusion happens almost simultaneously for different segments.

Evolution of Mean Conformation of Chain

If the random motion of the beads is averaged, we obtain the mean conformation of the sliding molecular chain. For each bead in the linear chain, Eq. (4) is used to expand the physical quantities into the linear combination of dynamic modes. Here we consider the mean conformation. Thus, by setting $f = \mathscr{X}(p, t)$ in Eq. (6a), the average value of the component $x(u, t)$ of the bead u on the linear chain can be solved as (details in **Appendix**):

$$\langle x(u,t)\rangle_x = \sum_{p=1}^{n_b}\sum_{q=1}^{n_b}\langle x(q,0)\rangle_x \zeta_u^{-1/2}\zeta_q^{1/2}V_{up}^x V_{qp}^x e^{-\lambda_p^x t} + \sum_{p=1}^{n_b}\zeta_u^{-1/2}\zeta_{n_b}^{-1/2}V_{up}^x V_{n_b p}^x \kappa^+ v_0 (\lambda_p^x)^{-2}(e^{-\lambda_p^x t} + \lambda_p^x t - 1) \quad (19a)$$

Similarly, in the y- and z-axis directions, there are

$$\langle y(u,t)\rangle_y = \sum_{p=1}^{n_b}\sum_{q=1}^{n_b}\langle y(q,0)\rangle_y \zeta_u^{-1/2}\zeta_q^{1/2}V_{up}^y V_{qp}^y e^{-\lambda_p^y t} + \sum_{p=1}^{n_b}\zeta_u^{-1/2}\zeta_{n_b}^{-1/2}V_{up}^y V_{n_b p}^y \kappa^+ y_0 (\lambda_p^y)^{-1}(1 - e^{-\lambda_p^y t}) \quad (19b)$$

$$\langle z(u,t)\rangle_z = \sum_{p=1}^{n_b}\sum_{q=1}^{n_b}\langle z(q,0)\rangle_z \zeta_u^{-1/2}\zeta_q^{1/2}V_{up}^z V_{qp}^z e^{-\lambda_p^z t} \quad (19c)$$

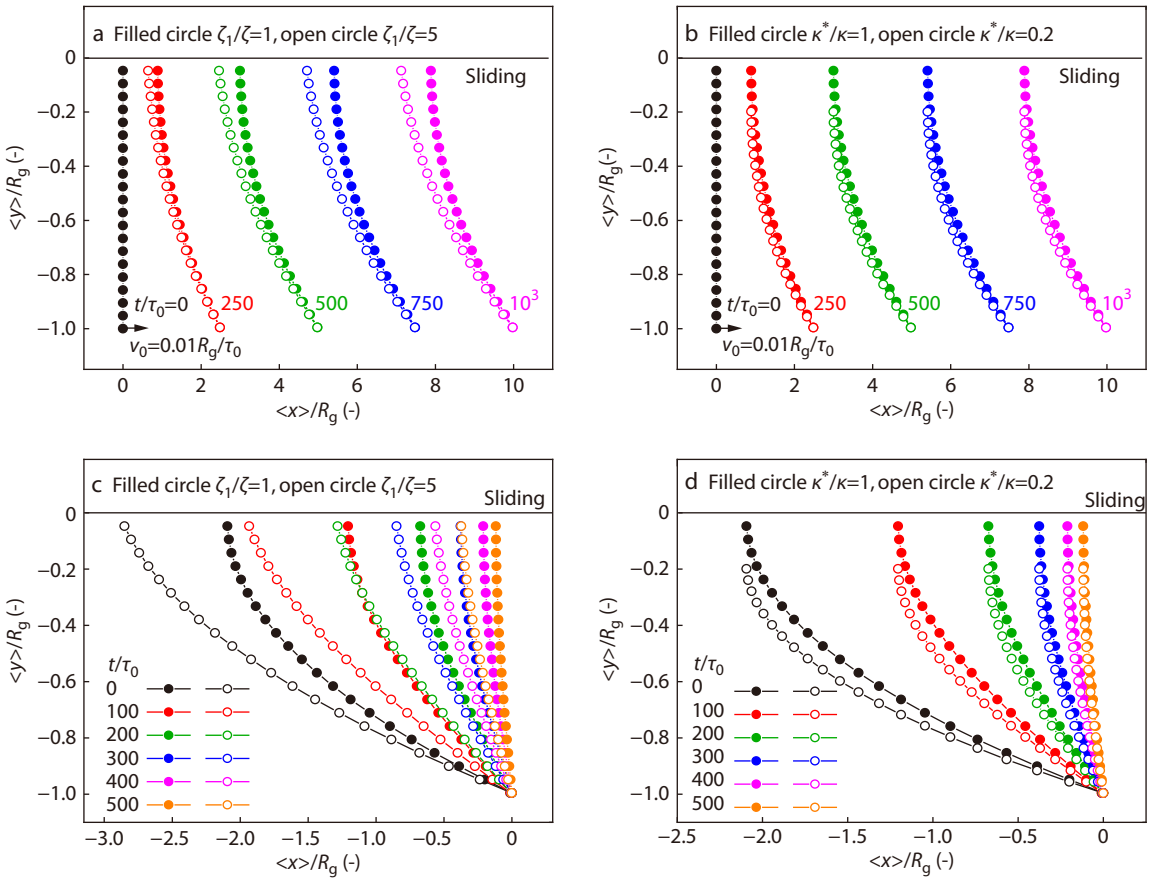

Fig. 7 The mean conformation of the polymer chain with chain end dragging: (a) different friction coefficients and (b) different constraint intensities of the sliding ring. The relaxation process after stopping dragging (v_0 = 0) when a steady state is reached. The mean conformation of the polymer chain with time during relaxation: (c) different friction coefficients and (d) different constraint intensities of the sliding ring. In the drag process, the intensity κ^+/κ = 10, the velocity $v_0 = 0.01R_g\tau_0^{-1}$, and the free end of the chain is stretched to $y_0/R_g = -1$, where R_g is the mean square radius of gyration of the whole chain, $\tau_0 = \zeta b^2/(3k_BT)$ is the basic relaxation time for a Kuhn unit.

where $\lambda_p^y = \lambda_p^z \neq 0, p = 1, 2, \cdots, n_b$.

For the free end $\kappa^+ = 0$, there is a zero eigenvalue $\lambda_{p^*}^x = 0$, and Eq. (19a) leads to

$$\langle x(u,t)\rangle_x = \mathrm{tr}^{-1}(\boldsymbol{\zeta})\sum_{q=1}^{n_b}\langle x(q,0)\rangle_x\zeta_q + \sum_{p=1,p\neq p^*}^{n_b}\sum_{q=1}^{n_b}\langle x(q,0)\rangle_x\zeta_u^{-1/2}\zeta_q^{1/2}V_{up}^xV_{qp}^xe^{-\lambda_p^xt} \tag{20}$$

where $V_{qp^*}^x$ is the q^{th} component of the eigenvector (Eq. 7) corresponding to the zero eigenvalue. For the free end shown in Fig. 2(a) with condition $\kappa^+ = 0$, the mean position $\langle \boldsymbol{R}(u,t)\rangle$ of each bead for a long time t becomes

$$\langle \boldsymbol{R}(u,t)\rangle|_{t\to\infty} = \left[\mathrm{tr}^{-1}(\boldsymbol{\zeta})\sum_{q=1}^{n_b}\langle x(q,0)\rangle_x\zeta_q, 0, 0\right] \tag{21}$$

It is shown that the mean position of the sliding bead eventually converges to the position of the center of mass of the whole linear chain (weighted by the friction coefficient) at the initial moment in the absence of the flow field. In the limit that all beads have the same friction, $\boldsymbol{\zeta} = \zeta\boldsymbol{\delta}$, when the sliding bead deviates from the position of the center of mass of the entire linear chain, Eq. (20) indicates that the sliding bead will slide along the fixed rod and eventually towards the projection point of the center of mass on the axis

$$\langle x(1,t)\rangle_x - \frac{1}{n_b}\sum_{q=1}^{n_b}\langle x(q,0)\rangle_x = \sum_{p=1,p\neq p^*}^{n_b}\cdot \sum_{q=1}^{n_b}\langle x(q,0)\rangle_x V_{1p}^xV_{qp}^xe^{-\lambda_p^xt} \tag{22}$$

where the sliding process is closely related to the initial conformation of the linear chain, *i.e.*, $\langle x(q,0)\rangle_x$, $q = 1, 2, \cdots, n_b$.

When dragging constraints exist with condition $\kappa^+ \neq 0$ (Fig. 2b), the time variation of the projection of the mean position of the polymer chain on the *xy*-plane can be calculated by Eqs. (19a) and (19b), and the results are shown in Fig. 7. To quantitatively describe the motion of the sliding ring with dragging at the chain end, we calculate the instantaneous velocity of the sliding ring (Fig. 8). The effect of friction coefficient, the constraint intensity, and the chain length are investigated. Figs. 7(a) and Fig. 8(a) compare the motion of the ring with different friction coefficients. Large friction coefficient $\zeta_1/\zeta = 5$ slows down the sliding motion of the ring, but does not influence the steady velocity, which equals the dragging speed. The constraint intensity of the ring κ^* does not affect the sliding velocity, as shown in Fig. 8(b), but affects the relative distance between the ring and the axial. The ring is pulled away from the axial when κ^* is much smaller than that of the polymer chain (Fig. 7b). As for the effect of polymer chain

https://doi.org/10.1007/s10118-023-2967-6

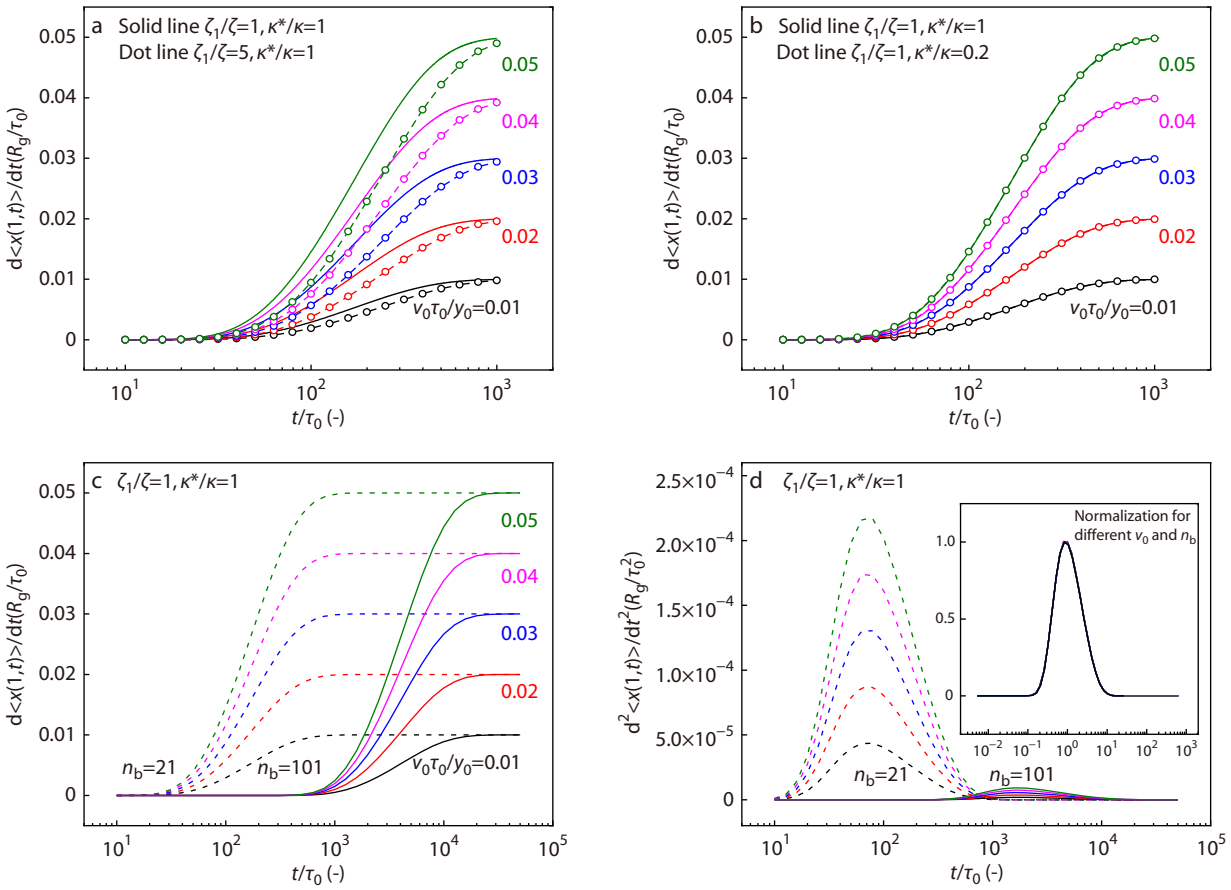

Fig. 8 Under the drag constraint, the instantaneous velocity of the sliding ring changes over time (n_b = 21): (a) effect of the friction coefficient of the sliding ring, (b) effect of the constraint intensity of the sliding ring, (c) the influence of chain lengths (n_b = 21 and n_b = 101), (d) the acceleration process of the sliding ring, and all the curves overlap after normalization (see the insert). The characteristic time (peak in d) is τ_{sr}/τ_0 = 79 for n_b = 21 and τ_{sr}/τ_0 = 1902 for n_b = 101.

length, the moment when the ring starts to move is delayed with the increase in molecular weight, but the process of ring acceleration is not related to the molecular chain length and the dragging speed. As shown in Fig. 8(d), the accelerations under different dragging speeds and chain lengths collapse into the normalized curves. Here we take the time corresponding to the maximum absolute value of acceleration as the characteristic time τ_{sr}. The characteristic time scale corresponding to a chain length of n_b = 21 is τ_{sr}/τ_0 = 79, while the characteristic time scale corresponding to n_b = 101 is τ_{sr}/τ_0 = 1902.

The relaxation process after stopping dragging (v_0 = 0) when a steady state is reached is shown in Figs. 7(c) and 7(d). The ring velocity and acceleration of sliding are shown in Fig. 9. Similar to the drag acceleration process, increasing the ring friction coefficient will slow down the sliding in the relaxation process. The effect of the sliding ring's confinement strength on the velocity is also insignificant. As for the effect of chain length, the moment when the ring starts to decelerate is also retarded for longer chains. Similarly, as shown in Fig. 9(d), the peak time of the deceleration is independent of the dragging speeds, and depends mainly on the chain length. Again, we define the peak time of deceleration as the characteristic time τ_{sr} of relaxation. The characteristic time scale corresponding to the chain length of n_b = 21 is τ_{sr}/τ_0 = 63, while the characteristic time scale corresponding to n_b = 101 is τ_{sr}/τ_0 = 1585. Note the characteristic time τ_{sr} is slightly faster in the retraction process than in the dragging process.

We further calculated the relationship between the characteristic time τ_{sr} and chain length. For comparison, the $\tau_{R,free}/\tau_0 = n_b^2/\left(2\pi^2\right)$ and $\tau_{R,constraint}/\tau_0$ are also plotted as a reference, where $\tau_{R,constraint}/\tau_0$ is calculated based on the dangling chain. It is clear that τ_{sr} increases with the ring friction coefficient, and is close to $\tau_{R,constraint}$ of a dangling chain when ζ_1/ζ_0 = 10. As shown in Fig. 10(a), a simple power law relation is seen with the scaling exponent slightly influenced by the heterogeneity of the sliding ring friction coefficient, but without any significant dependence on the heterogeneity of the constraint intensity. With the increase of the friction of the sliding ring, the scaling exponent shown in Fig. 10(a) decreases from 2 for homogeneous friction (ζ_1/ζ_0 = 1) to about 1.85 for the ring with very large friction coefficient (ζ_1/ζ_0 = 10). Similar phenomenon is observed for the characteristic time of the recovery process (Fig. 10b). It is shown that the start drag acceleration process and the recovery process after steady-state sliding exhibit the same relaxation behavior of the chain segments. Comparison between τ_{sr} and $\tau_{R,free}$ is shown in Fig. 10(c). The τ_{sr} is about three times larger than

https://doi.org/10.1007/s10118-023-2967-6

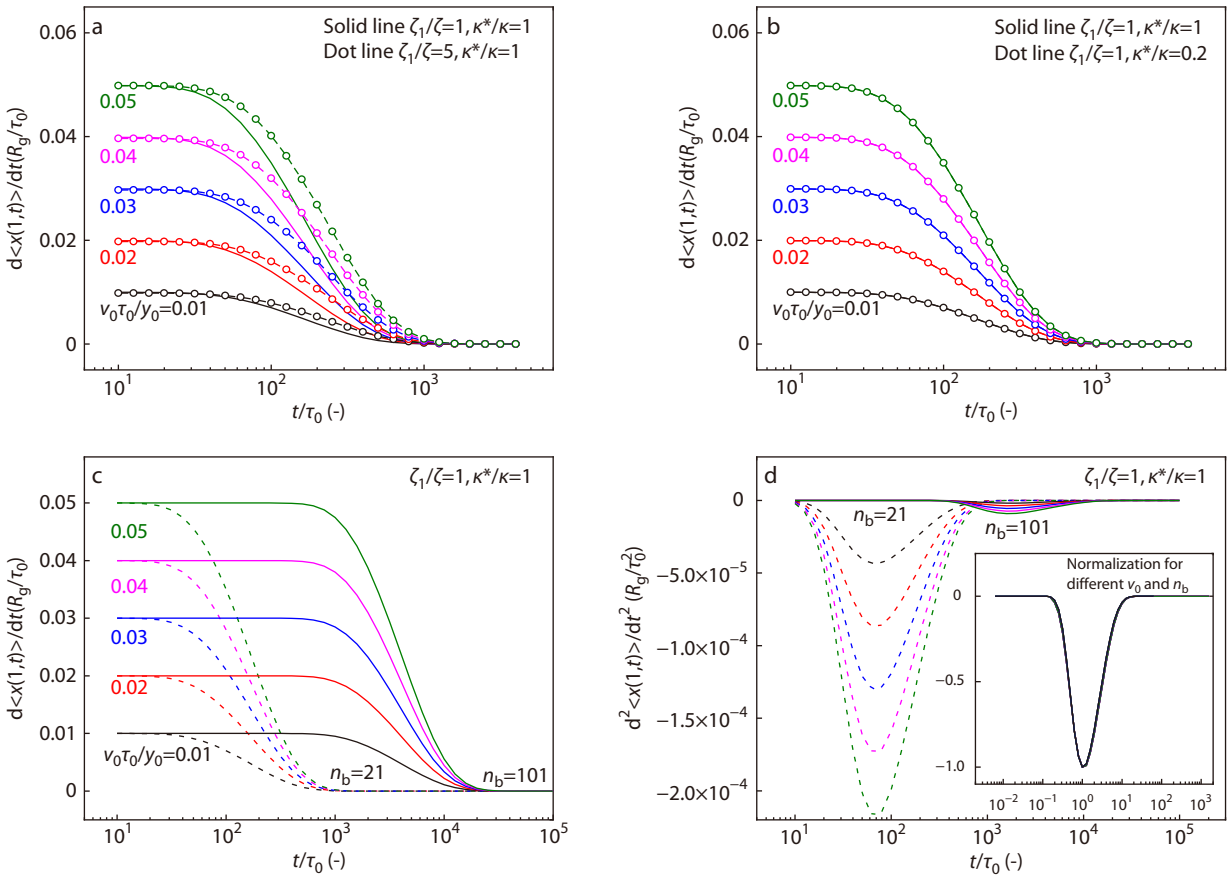

Fig. 9 The instantaneous velocity of the sliding ring during the relaxation process without dragging after reaching a steady state under drag constraints (n_b = 21): (a) effect of the friction coefficient of the sliding ring, (b) effect of the constraint intensity of the sliding ring, (c) the influence of chain lengths (n_b = 21 and n_b = 101), (d) the acceleration process of the sliding ring, and all the curves overlap after normalization (see the insert). The characteristic time (peak in d) is τ_{sr}/τ_0 = 63 for n_b = 21 and τ_{sr}/τ_0 = 1585 for n_b = 101.

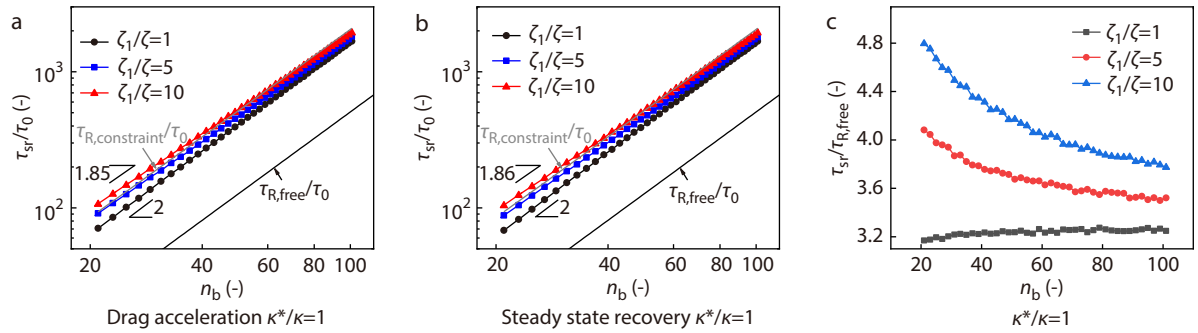

Fig. 10 The relationship between the characteristic time τ_{sr} and the chain length: (a) the drag acceleration process under start-up, (b) the steady state recovery process after stopping dragging. (c) $\tau_{sr}/\tau_{R,free}$ as a function of chain length for different sliding ring frictions. Both processes (a) and (b) exhibit the same relaxation behavior of the sliding chain. τ_{sr} is the time corresponding to the maximal absolute value of the acceleration.

$\tau_{R,free}$ and almost independent of chain length for homogeneous friction (ζ_1/ζ_0 = 1). As the friction coefficient of the sliding ring increases, $\tau_{sr}/\tau_{R,free}$ decreases with the chain length, and becomes a constant if the chain is sufficient long (yet not entangled).

As shown in Eq. (22), the sliding process strongly correlates with the initial chain conformation. To illustrate this, we also calculate the relaxation of the chain by sliding after a step deformation, where the polymer chain is assumed to deform affinely into a straight chain conformation. The results are shown in Fig. 11. The difference between Figs. 11(a) and 11(b) and Figs. 7(c) and 7(d) is that the initial conformation of the chain is different. The instantaneous velocity of the sliding ring during relaxation is shown in Fig. 12 for the affine conformation. In contrast to the relaxation after dragging (Fig. 9), the relaxation of the affine conformation after a fast step deformation shows two distinct relaxation processes, a fast one and a slow one, as shown in Fig. 12. The fast relaxation pro-

https://doi.org/10.1007/s10118-023-2967-6

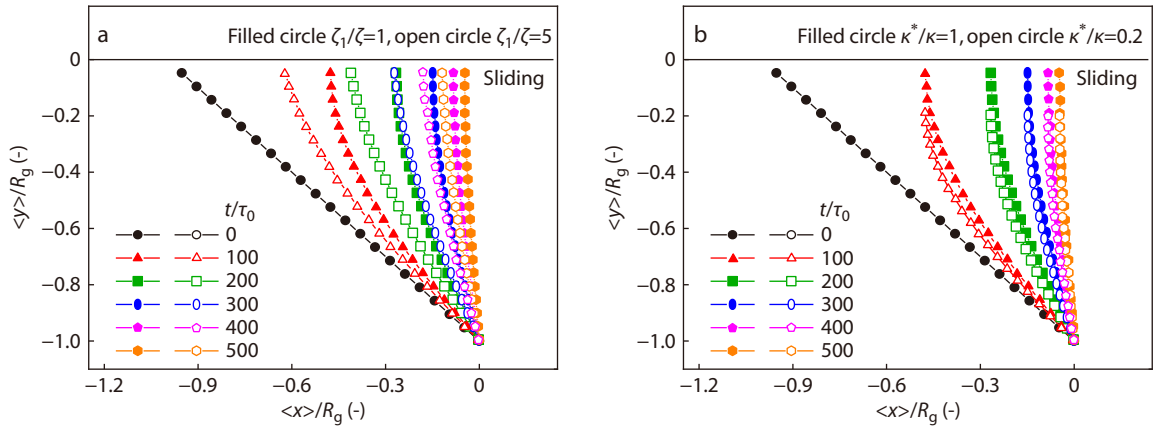

Fig. 11 The average conformation evolution of the polymer chain after step deformation (affine conformation) with fixed constraint intensity $\kappa^+/\kappa = 10$, where the sliding ring is stretched to $x_0/R_g = -1$, and the free end is stretched to $y_0/R_g = -1$. The coordinate unit is R_g. (a) Effect of friction coefficients of the sliding ring, (b) effect of constraint intensity of the sliding ring.

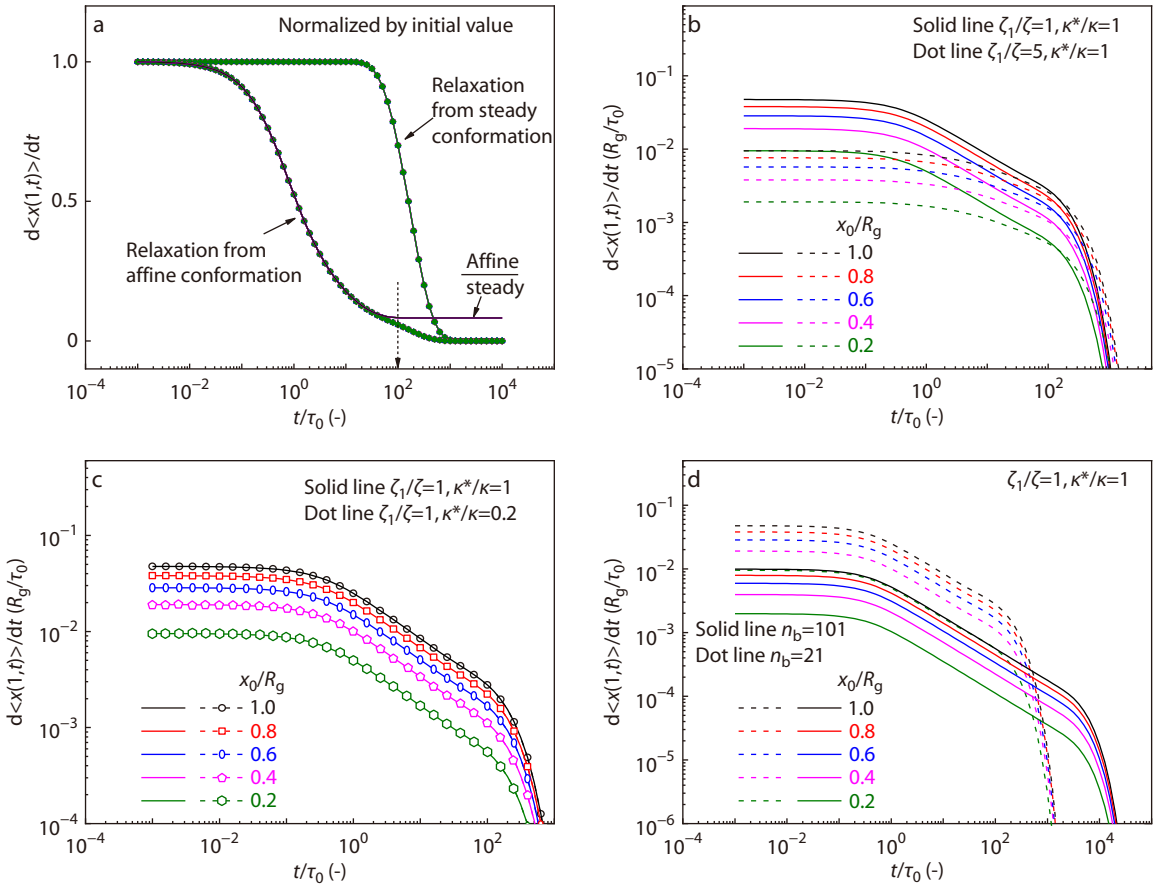

Fig. 12 The instantaneous velocity of the sliding ring during relaxation after step deformation under fixed constraints. (a) Comparison of different relaxation processes: relaxation after dragging (steady conformation) versus relaxation after step deformation (affine conformation); (b) Effect of friction coeffect of the sliding ring, (c) effect of constraint intensity of the sliding ring, (d) effect of chain length (n_b = 21 and n_b = 101).

cess starts at the relaxation time scale $t/\tau_0 \approx 1$ (corresponding to one Kuhn unit scale), and span up to the whole chain relaxation time scale. The whole chain relaxation time corresponds to the mean square end-to-end distance scale of the whole chain, which can be identified from the time at the bifurcation of MSD in Fig. 4(e) for chain length n_b = 21 with $t/\tau_0 \approx 100$, and from Fig. 5(a) for chain length n_b = 101 with $t/\tau_0 \approx 3000$. After the fast relaxation process is completed, the second relaxation process is similar to the sliding relaxation process, which can be seen from the constant ratio of affine conformation and steady conformation in Fig. 12(a) after the whole chain relaxation time scale. It indicates that the

https://doi.org/10.1007/s10118-023-2967-6

molecular chain has lost its memory for the initial conformation after the relaxation time scale corresponding to the whole chain mean square end-to-end distance scale. In addition, if the friction of the sliding ring increases, the initial velocity will be smaller, and the relaxation behaves similarly (Fig. 12b), but there is no significant dependency on the constraint intensity of the sliding ring (Fig. 12c). With the increasing of chain length, the fast relaxation process becomes longer, which is because of the larger mean square end-to-end distance. All these results imply an additional sliding process in the relaxation of sliding chains after deformation, which is evidently slower than the terminal relaxation of the corresponding free chain.

CONCLUSIONS

In this work, we model the sliding confinement in the sliding ring materials to understand the sliding dynamics from the viewpoint of bead-spring chains. The motion of the chain segment subject to sliding constraints is the key feature that makes it different from polymers with monomers connected by covalent bonds or dynamic bonds. Based on the heterogeneous bead-spring (HBS) model, we further extend the local homogeneous constraints to direction-dependent constraints, which define the sliding constraints to capture the main features of the sliding motions. The diffusion behavior and the evolution of the mean conformation of the polymer chain attached to the sliding ring in the presence of drag can be captured quantitatively by the present sliding ring model. A slow mode is observed in the diffusion of segments and in the response to the loading/unloading of external stimuli. By comparing with the dynamics of free chains, dangling chains and network strands, this slow mode is ascribed to the sliding motion of the ring. These results are helpful for identifying the sliding motion in rotaxane-based mechanically interlocked polymers, including the sliding ring gels.

APPENDIX

Solution of the Conformation Evolution Equation of Sliding Chain

(1) The evolution of the mean conformation.

By setting $f = \mathcal{X}(p,t)$, $\mathcal{Y}(p,t)$, or $\mathcal{Z}(p,t)$ respectively in Eq. (6), we have

$$\frac{\partial\langle\mathcal{X}(p,t)\rangle_x}{\partial t} = -\lambda_p^x\langle\mathcal{X}(p,t)\rangle_x + \zeta_{n_b}^{-1/2}V_{n_b p}^x\kappa^+ v_0 t \tag{23a}$$

$$\frac{\partial\langle\mathcal{Y}(p,t)\rangle_y}{\partial t} = -\lambda_p^y\langle\mathcal{Y}(p,t)\rangle_y + \zeta_{n_b}^{-1/2}V_{n_b p}^y\kappa^+ y_0 \tag{23b}$$

$$\frac{\partial\langle\mathcal{Z}(p,t)\rangle_z}{\partial t} = -\lambda_p^z\langle\mathcal{Z}(p,t)\rangle_z \tag{23c}$$

with the solution

$$\langle\mathcal{X}(p,t)\rangle_x = e^{-\lambda_p^x t}\langle\mathcal{X}(p,0)\rangle_x + \zeta_{n_b}^{-1/2}V_{n_b p}^x\kappa^+ v_0\left(\lambda_p^x\right)^{-2}\left(e^{-\lambda_p^x t} + \lambda_p^x t - 1\right) \tag{24a}$$

$$\langle\mathcal{Y}(p,t)\rangle_y = e^{-\lambda_p^y t}\langle\mathcal{Y}(p,0)\rangle_y + \zeta_{n_b}^{-1/2}V_{n_b p}^y\kappa^+ y_0\left(\lambda_p^y\right)^{-1}\left(1 - e^{-\lambda_p^y t}\right) \tag{24b}$$

$$\langle\mathcal{Z}(p,t)\rangle_z = e^{-\lambda_p^z t}\langle\mathcal{Z}(p,0)\rangle_z \tag{24c}$$

where $p = 1, 2, \cdots, n_b$. This is true for condition $\kappa^+ = 0$, where there is a zero eigenvalue. By the initial condition $\langle\boldsymbol{R}(t)\rangle|_{t=0} = \left[\langle\boldsymbol{x}(0)\rangle_x, \langle\boldsymbol{y}(0)\rangle_y, \langle\boldsymbol{z}(0)\rangle_z\right]$ to determine the undetermined coefficient

$$\langle\mathcal{X}(0)\rangle_x = \left(\boldsymbol{V}^x\right)^T\cdot\boldsymbol{\zeta}^{1/2}\cdot\langle\boldsymbol{x}(0)\rangle_x \tag{25a}$$

$$\langle\mathcal{Y}(0)\rangle_y = \left(\boldsymbol{V}^y\right)^T\cdot\boldsymbol{\zeta}^{1/2}\cdot\langle\boldsymbol{y}(0)\rangle_y \tag{25b}$$

$$\langle\mathcal{Z}(0)\rangle_z = \left(\boldsymbol{V}^z\right)^T\cdot\boldsymbol{\zeta}^{1/2}\cdot\langle\boldsymbol{z}(0)\rangle_z \tag{25c}$$

Combined with Eqs. (4), (24) and (25), the evolution of the average position of each bead is thus obtained.

(2) The evolution of the correlation of the dynamic modes.

Set $f = \mathcal{X}^2(p,t)$ and substitute it into Eq. (6a), we get

$$\frac{\partial\left\langle\mathcal{X}^2(p,t)\right\rangle_x}{\partial t} = -2\lambda_p^x\left\langle\mathcal{X}^2(p,t)\right\rangle_x + 2k_BT \tag{26}$$

Thus, for $\lambda_p^x \neq 0$, we get

$$\left\langle\mathcal{X}^2(p,t)\right\rangle_x = \left(\left\langle\mathcal{X}^2(p,0)\right\rangle_x - \frac{k_BT}{\lambda_p^x}\right)e^{-2\lambda_p^x t} + \frac{k_BT}{\lambda_p^x} \tag{27a}$$

and for $\lambda_{p^*}^x = 0$, we get

$$\left\langle\mathcal{X}^2(p^*,t)\right\rangle_x = \left\langle\mathcal{X}^2(p^*,0)\right\rangle_x + 2k_BTt \tag{27b}$$

Eq. (27b) describes the translational diffusion mode in the x-axis direction. Thus, Eq. (10a) for $u = v$ reduces to

$$\left\langle x^2(u,t)\right\rangle_x = \mathrm{tr}^{-1}(\boldsymbol{\zeta})\left\langle\mathcal{X}^2(p^*,t)\right\rangle_x + \zeta_u^{-1}\sum_{p=1,p\neq p^*}^{n_b}V_{up}^xV_{up}^x\left\langle\mathcal{X}^2(p,t)\right\rangle_x \tag{28}$$

by utilizing the eigenvector corresponding to the zero eigenvalue (Eq. 7), and $\left\langle\mathcal{X}^2(p,t)\right\rangle_x$ and $\left\langle\mathcal{X}^2(p^*,t)\right\rangle_x$ are determined by Eq. (27). Set $f = \mathcal{X}(p,t)\mathcal{X}(q,0)$, and substitute into Eq. (6a) to get

$$\frac{\partial\langle\mathcal{X}(p,t)\mathcal{X}(q,0)\rangle_x}{\partial t} = -\lambda_p^x\langle\mathcal{X}(p,t)\mathcal{X}(q,0)\rangle_x \tag{29}$$

The solution is

$$\langle\mathcal{X}(p,t)\mathcal{X}(q,0)\rangle_x = \delta_{pq}\left\langle\mathcal{X}^2(p,0)\right\rangle_x e^{-\lambda_p^x t} \tag{30}$$

Thus,

$$\langle x(u,t)x(u,0)\rangle_x = \mathrm{tr}^{-1}(\boldsymbol{\zeta})\left\langle\mathcal{X}^2(p^*,0)\right\rangle_x + \zeta_u^{-1}\sum_{p=1,p\neq p^*}^{n_b}V_{up}^xV_{up}^x\left\langle\mathcal{X}^2(p,0)\right\rangle_x e^{-\lambda_p^x t} \tag{31}$$

The result is obtained by definition Eq. (8a) $\left\langle(x(u,t)-x(u,0))^2\right\rangle_x = \left\langle x^2(u,t)\right\rangle_x + \left\langle x^2(u,0)\right\rangle_x - 2\langle x(u,t)x(u,0)\rangle_x$. Similarly, set $f = \mathcal{Y}^2(p,t)$ and $\mathcal{Z}^2(p,t)$, and substitute them into Eqs. (6b) and (6c), respectively, we get

$$\frac{\partial\left\langle\mathcal{Y}^2(p,t)\right\rangle_y}{\partial t} = -2\lambda_p^y\left\langle\mathcal{Y}^2(p,t)\right\rangle_y + 2k_BT \tag{32a}$$

$$\frac{\partial\left\langle\mathcal{Z}^2(p,t)\right\rangle_z}{\partial t} = -2\lambda_p^z\left\langle\mathcal{Z}^2(p,t)\right\rangle_z + 2k_BT \tag{32b}$$

The solutions are

$$\left\langle\mathcal{Y}^2(p,t)\right\rangle_y = \left(\left\langle\mathcal{Y}^2(p,0)\right\rangle_y - \frac{k_BT}{\lambda_p^y}\right)e^{-2\lambda_p^y t} + \frac{k_BT}{\lambda_p^y} \tag{33a}$$

$$\left\langle\mathcal{Z}^2(p,t)\right\rangle_z = \left(\left\langle\mathcal{Z}^2(p,0)\right\rangle_z - \frac{k_BT}{\lambda_p^z}\right)e^{-2\lambda_p^z t} + \frac{k_BT}{\lambda_p^z} \tag{33b}$$

https://doi.org/10.1007/s10118-023-2967-6

Since $\lambda_p^y = \lambda_p^z \neq 0$, there is no translational diffusion mode in the y- and z-axis directions anymore. Then set $f = \mathcal{Y}(p,t)\mathcal{Y}(q,0)$ and $\mathcal{Z}(p,t)\mathcal{Z}(q,0)$, and substitute into Eqs. (6b) and (6c), we get

$$\frac{\partial\langle\mathcal{Y}(p,t)\mathcal{Y}(q,0)\rangle_y}{\partial t} = -\lambda_p^y\langle\mathcal{Y}(p,t)\mathcal{Y}(q,0)\rangle_y \tag{34a}$$

$$\frac{\partial\langle\mathcal{Z}(p,t)\mathcal{Z}(q,0)\rangle_z}{\partial t} = -\lambda_p^z\langle\mathcal{Z}(p,t)\mathcal{Z}(q,0)\rangle_z \tag{34b}$$

The solutions are

$$\langle\mathcal{Y}(p,t)\mathcal{Y}(q,0)\rangle_y = \delta_{pq}\left\langle\mathcal{Y}^2(p,0)\right\rangle_y e^{-\lambda_p^y t} \tag{35a}$$

$$\langle\mathcal{Z}(p,t)\mathcal{Z}(q,0)\rangle_z = \delta_{pq}\left\langle\mathcal{Z}^2(p,0)\right\rangle_z e^{-\lambda_p^z t} \tag{35b}$$

Conflict of Interests

The authors declare no interest conflict.

ACKNOWLEDGMENTS

This work was financially supported by the National Natural Science Foundation of China (Nos. 51625303 and 21790344).

REFERENCES

1 Gurtovenko, A.; Blumen, A. Generalized Gaussian structures: models for polymer systems with complex topologies. *Adv. Polym. Sci.* **2005**, *182*, 171–282.
2 Xiong, Z.; Yu, W. Molecular constitutive equation for unentangled branch copolymers. *Rheol. Acta* **2021**, *60*, 439–455.
3 Doi, M.; Edwards, S. F. The theory of polymer dynamics. *Oxford University Press* **1986**.
4 Xiong, Z.; Yu, W. An orientation-stretch coupled model for entangled comb polymers. *J. Rheol.* **2021**, *65*, 113–128.
5 Xiong, Z.; Yu, W. A nonlinear constitutive model for entangled symmetric dendrimers. *J. Rheol.* **2022**, *66*, 907–923.
6 Pratchayanan, D.; Yang, J. C.; Lewis, C. L.; Thoppey, N.; Anthamatten, M. Thermomechanical insight into the reconfiguration of Diels-Alder networks. *J. Rheol.* **2017**, *61*, 1359–1367.
7 Cheng, L.; Zhao, X.; Zhao, J.; Liu, S.; Yu, W. Structure and dynamics of associative exchange dynamic polymer networks. *Macromolecules* **2022**, *55*, 6598–6608.
8 Kato, K.; Karube, K.; Nakamura, N.; Ito, K. The effect of ring size on the mechanical relaxation dynamics of polyrotaxane gels. *Polym. Chem.* **2015**, *6*, 2241–2248.
9 Kato, K.; Yasuda, T.; Ito, K. Viscoelastic properties of slide-ring gels reflecting sliding dynamics of partial chains and entropy of ring components. *Macromolecules* **2013**, *46*, 310–316.
10 Momčilović, N.; Clark, P. G.; Boydston, A. J.; Grubbs, R. H. One-pot synthesis of polyrotaxanes *via* acyclic diene metathesis polymerization of supramolecular monomers. *J. Am. Chem. Soc.* **2011**, *133*, 19087–19089.
11 Wang, Y. C.; Maeda, R.; Kali, G.; Yokoyama, H.; Wenz, G.; Ito, K. Synthesis of poly(methyl methacrylate)-based polyrotaxane *via* reversible addition-fragmentation chain transfer polymerization. *ACS Macro. Lett.* **2020**, *9*, 1853–1857.
12 Ito, K. Novel entropic elasticity of polymeric materials: why is slide-ring gel so soft. *Polym. J.* **2012**, *44*, 38–41.
13 Lu, Y.; Aoki, D.; Sawada, J.; Kosuge, T.; Sogawa, H.; Otsuka, H.; Takata, T. Visualization of the slide-ring effect: a study on movable crosslinking points using mechanochromism. *Chem. Commun.* **2020**, *56*, 3361–3364.
14 Liu, C.; Kadono, H.; Mayumi, K.; Kato, K.; Yokoyama, H.; Ito, K. Unusual fracture behavior of slide-ring gels with movable crosslinks. *ACS Macro. Lett.* **2017**, *6*, 1409–1413.
15 Yang, X.; Cheng, L.; Zhang, Z.; Zhao, J.; Bai, R.; Guo, Z.; Yu, W.; Yan, X. Amplification of integrated microscopic motions of high-density [2]rotaxanes in mechanically interlocked networks. *Nat. Commun.* **2022**, *13*, 6654.
16 Zhang, Z.; Zhao, J.; Guo, Z.; Zhang, H.; Pan, H.; Wu, Q.; You, W.; Yu, W.; Yan, X. Mechanically interlocked networks crosslinked by a molecular necklace. *Nat. Commun.* **2022**, *13*, 1393.
17 Zhao, J.; Zhang, Z.; Cheng, L.; Bai, R.; Zhao, D.; Wang, Y.; Yu, W.; Yan, X. Mechanically interlocked vitrimers. *J. Am. Chem. Soc.* **2022**, *144*, 872–882.
18 Zhang, Z.; You, W.; Li, P.; Zhao, J.; Guo, Z.; Xu, T.; Chen, J.; Yu, W.; Yan, X. Insights into the correlation of microscopic motions of [c2]daisy chains with macroscopic mechanical performance for mechanically interlocked networks. *J. Am. Chem. Soc.* **2023**, *145*, 567–578.
19 Yan, Z.; Ye, L.; Zhang, A. Y.; Feng, Z. G. The mobility of threaded α-cyclodextrins in PR copolymer and its influences on mechanical properties. *Chinese. J. Polym. Sci.* **2017**, *35*, 752–763.
20 Kato, K.; Ohara, A.; Michishio, K.; Ito, K. Effects of ring size on the dynamics of polyrotaxane glass. *Macromolecules* **2020**, *53*, 8910–8917.
21 Kashiwagi, Y.; Urakawa, O.; Zhao, S.; Takashima, Y.; Harada, A.; Inoue, T. Dynamics of the topological network formed by movable crosslinks: effect of sliding motion on dielectric and viscoelastic relaxation behavior. *Macromolecules* **2021**, *54*, 3321–3333.
22 Yasuda, Y.; Toda, M.; Mayumi, K.; Yokoyama, H.; Morita, H.; Ito, K. Sliding dynamics of ring on polymer in rotaxane: a coarse-grained molecular dynamics simulation study. *Macromolecules* **2019**, *52*, 3787–3793.
23 Li, K.; Wang, Y.; Guo, F.; He, L.; Zhang, L. Sliding dynamics of multi-rings on a semiflexible polymer in poly[n]catenanes. *Soft. Matter.* **2021**, *17*, 2557–2567.
24 Guo, F.; Li, K.; Wu, J.; Wang, Y.; Zhang, L. Sliding dynamics of ring chain on a knotted polymer in rotaxane. *Polymer* **2021**, *235*, 124226.
25 Zhang, Z.; Hou, G.; Shen, J.; Liu, J.; Gao, Y.; Zhao, X.; Zhang, L. Designing the slide-ring polymer network with both good mechanical and damping properties *via* molecular dynamics simulation. *Polymers* **2018**, *10*, 964.
26 Wu, J.; Guo, F.; Li, K.; Zhang, L. Sliding dynamics of ring chains on two asymmetric/symmetric chains in a simple slide-ring gel. *Polymers* **2022**, *14*, 79.
27 Yasuda, Y.; Hidaka, Y.; Mayumi, K.; Yamada, T.; Fujimoto, K.; Okazaki, S.; Yokoyama, H.; Ito, K. Molecular dynamics of polyrotaxane in solution investigated by quasi-elastic neutron scattering and molecular dynamics simulation: sliding motion of rings on polymer. *J. Am. Chem. Soc.* **2019**, *141*, 9655–9663.
28 Vernerey, F. J.; Lamont, S. Transient mechanics of slide-ring networks: A continuum model. *J. Mech. Phys. Solids* **2021**, *146*, 104212.
29 Vernerey, F. J.; Long, R.; Brighenti, R. A statistically-based continuum theory for polymers with transient networks. *J. Mech. Phys. Solids* **2017**, *107*, 1–20.
30 Shang, C.; Xiong, Z.; Liu, S.; Yu, W. Molecular dynamics of azobenzene polymer with photoreversible glass transition. *Macromolecules* **2022**, *55*, 3711–3722.